Texturing hierarchical tissues by gradient assembling of microengineered platelet-lysates activated fibers

Isabel Calejo, Rui L. Reis, Rui M. A. Domingues, Manuela E. Gomes**

I. Calejo, Prof. R. L. Reis, Dr. Rui M. A. Domingues, Prof. M. E. Gomes

3B's Research Group, i3Bs – Research Institute on Biomaterials,

Biodegradables and Biomimetics

University of Minho4805-017 Barco, Guimarães, Portugal

E-mail: rui.domingues@i3bs.uminho.pt; megomes@i3bs.uminho.pt

Keywords

Emulsion Electrospinning; Functionally graded scaffolds; Platelet lysates; Hierarchical tissues

Abstract

The heterogeneity of the hierarchical tissues requires designing multipart engineered constructs as suitable tissue replacements. Herein, we propose the incorporation of platelet lysate (PL) within electrospun fiber core aiming the fabrication of functionally graded 3D scaffolds for heterotypic tissues regeneration, such as tendon-to-bone interface. First, anisotropic yarns (A-Yarns) and isotropic threads with nanohydroxyapatite (I-Threads/PL@nHAp) are fabricated to recreate the

This article has been accepted for publication and undergone full peer review but has not been through the copyediting, typesetting, pagination and proofreading process, which may lead to differences between this version and the Version of Record. Please cite this article as doi: 10.1002/adhm.202102076.

tendon- and bone- microstructures and both incorporated with PL using emulsion electrospinning for a sustained and local delivery of growth factors, cytokines, and chemokines. Biological performance using human adipose-derived stem cells demonstrates that A-Yarns/PL induce a higher expression of scleraxis, a tenogenic-marker, while in I-Threads/PL@nHAp, higher alkaline phosphatase activity and matrix mineralization suggest an osteogenic commitment without the need for external biochemical supplementation when compared to plain controls. As proof of concept, functional 3D gradient scaffolds are fabricated using weaving technique, resulting in 3D textured hierarchical constructs with gradients in composition and topography. Additionally, the precise delivery of bioactive cues together with *in situ* biophysical features guide the commitment into a phenotypic gradient exhibiting chondrogenic and osteochondrogenic profiles in the interface of scaffolds. Overall, we demonstrate a promising patch solution for the regeneration of tendon-to-bone tissue interface through the fabrication of PL-functional 3D gradient constructs.

1.Introduction

Musculoskeletal hierarchical tissues pathologies are still a clinical burden due to their complexity. For instance, the tendon-to-bone interface is divided into four continuous zones – tendon, mineralized-, non-mineralized fibrocartilage, and bone - composed of various cell types and extracellular matrix (ECM) composition, resulting in a structural and compositional gradient, reflected in its capacity of load-bearing[1]. Injuries are highly prevalent, and currently used tissue-grafts face several significant shortcomings, such as adverse host tissue reaction, donor site morbidity, and formation of neofibrovascular tissue, compromising graft integrity[1a, 2] and resulting in high re-tear rates[3]. Therefore, considering tendon-to-bone interface complexity, there is a need to develop improved systems that meet the biophysical, biochemical, and mechanical requirements of this highly heterotypic tissue, generating suitable tissue replacements.

In this regard, functionally graded materials (FGMs) have been presented as promising scaffolds in the field of tissue engineering, designed to mimic native gradients in composition, structure,

mechanical properties, and signaling cues found in the native tissue[4]. With an increasing use of FGMs in tissue engineering, fiber-based systems have been used as building blocks of biotextiles, playing an essential role in controlling a myriad of properties of resulting 3D gradient constructs. Thus, several technologies have been developed for the fabrication of synthetic and natural fibrous biomaterials, namely microfluidics[5], melt spinning[6], wet-spinning[7] and electrospinning[8]. Electrospinning is one of the most widely used techniques, mainly due to its relative simplicity, efficient control over processing parameters, scaling up possibility, and practicability to fabricate micro/nanosized fibers with ECM-like structure[9]. For example, our group recently reported the fabrication of continuous electrospun anisotropic nanofibers threads that were then hierarchically assembled by textile into 3D scaffolds recreating the fibrillar hierarchical organization and topography of tendon tissues[10]. Similarly, Moffat et al. demonstrated the capability of isotropic nanofiber poly(lactic-co-glycolic acid) (PLGA) scaffolds to induce human rotator cuff fibroblasts attachment and deposition of collagenous matrix according to substrate orientation[11]. Other multilayered scaffolds and multiscale mesh waves have also been produced using similar electrospinning or 3D printing systems, aiming at replicating the organization and fibers orientation of complex tissues [12]. Yet, previously reported fiber/scaffolds units still fail in to incorporate and/or release important biological factors for cell signaling in a controlled spatiotemporal manner. Thus, different materials engineering approaches for the incorporation of drugs and bioactive molecules within fibers have been investigated over the years, particularly exploring fabrication methods such as coaxial electrospinning[13]. This technique relies on the production of core-shell structures, in which two solutions can be coaxially and simultaneously electrospun by different capillary channels, enabling the incorporation of bioactive molecules within fibers[14]. However, besides the inherent complexity associated with its setup, several parameters, including apparatus design, flow rate of the inner and outer solutions, as well as their viscoelasticity and interfacial tension, need to be considered since they can affect the entrainment and production of required core-shell fiber morphology[15]. Alternatively, emulsion electrospinning has gained attention as a suitable substitute to overcome these problems, especially using water-in-oil emulsions. Under electric force, the emulsion containing the polymeric solution and the water phase made of sub- to micron-spheres is elongated and converted into core-shell structure fibers[16], enabling an easy and continuous incorporation of biomolecules into electrospun fibers core. Thus, raising the potential application of

this fabrication technique for the development of functionally graded materials for hierarchical tissues, such as tendon-to-bone interface, through the integration of both biological, biochemical and tissue engineered cues, shall enable the regeneration of injured tissue interfaces by the local and controlled release of biochemical factors and consequent deposition of architecturally oriented ECM.

Biological factors can play a significant role in tissue healing, as cellular activities are regulated by a panoply of growth factors (GFs), cytokines, and chemokines. Therefore, over the years, several material and drug delivery engineering strategies have proposed the encapsulation of biomolecules into fibrous constructs and theirs subsequent controlled release to achieve specific therapeutic effects in the targeted microenvironments[17]. However, despite different biomolecules have been encapsulated into core-shell fibers through co-electrospinning[18], the proposed strategies frequently rely on single GF encapsulation, while tissue healing is a finely orchestrated process involving multiple signaling biomolecules, thus limiting the therapeutic potential of these biomaterials. Moreover, the high costs of recombinant GFs and the difficulty of adequately controlling its programmed release kinetics to match the healing time are other major limitations hindering the implementation of such strategies[19]. The use of platelet lysates (PLs) as an alternative to recombinant GFs might contribute to overcome some of these issues. This biomolecule cocktail can be obtained through cost-effective and straightforward protocols[20], has numerous bioactive components, including GFs with known important roles in several biological processes (e.g., cell adhesion, proliferation, and differentiation) and proved efficiency on promoting tissue healing and regeneration[20b, 21]. As an example, PDGF, FGF, VEGF and TGF-ß have shown, by different effects, to accelerate interfacial healing and enhance the insertional strength of tendon grafts both *in vitro* and *in vivo* models[22]. Further, chemokines such as RANTES and CXCL1 have been described to have a potential role in fracture repair and tendon healing, mainly associated with inflammatory response and macrophages recruitment[23]. Currently, particular emphasis is given to strategies that enable to control their spatiotemporal delivery and improve the selectivity of presentation profiles of growth factors derived from PL. Therefore, the development of advanced functional and controllable systems, through the coupling of biological factors release with advanced tissue engineered strategies, might enable the development of functional systems for the in-situ delivery of well

characterized populations of biomolecules improving the therapeutic efficiency during healing phases.

Building on the concept of functional graded materials, we fabricated PL-biofunctionalized fibers with different topographical features to recapitulate the native architecture of hierarchical tissues, while enabling the precise and controlled release of biological molecules important for tissues regeneration. To that end, emulsion electrospinning was used for the incorporation of biological factors (PLs) in polycaprolactone (PCL) nanofiber threads with two different topographies, anisotropic and isotropic. Anisotropic fiber threads were hierarchically assembled into yarns (A-Yarn/PL) to replicate tendon's architecture, while isotropic threads (I-Thread/PL) were incorporated with nHAp to mimic bone's organic phase and organization. Beyond recreating the architecture of different tissues, the release profile of encapsulated PL bioactive components was assessed, mainly focusing on the delivery kinetics of GFs, cytokines and chemokines under healthy (physiological) and injured (inflammatory) conditions. To clearly understand the temporal combinatory effect of topography and biomolecules release over stem cell phenotype commitment, human adipose-derived stem cells (hASCs) were seeded on A-Yarn/PL and I-Thread/PL. Finally, as a proof-of-concept, textile techniques were applied for the fabrication 3D functionally graded constructs with spatially distributed gradients of architecture, topography, biological and biochemical composition that characterize the hierarchical tissue, namely the native tendon-to-bone interface. Overall, the developed approach holds great promise for the fabrication of 3D functional gradient scaffolds through easy and scalable techniques for tendon-to-bone tissue integration and proper regeneration.

2. Results and Discussion

2.1. Fabrication of electrospun fiber threads with different surface topographies

Within every tissue, the properties of cell's supporting environment are sensed at multiple length scales. Interestingly, the conjugation of tissue-generated forces at the macroscale with cellular forces at the microscale, are paramount for guiding multi-cell differentiation during development,

particularly on musculoskeletal tissues[24]. For instance, stem cell lineage specification can be governed by the physical contact with specific architectures of the surrounding microenvironment[25]. As previously reported, the topography of electrospun fibers plays an important role in maintaining and inducing a specific phenotype in stem cells[8a, 26]. In this work, textured electrospun fiber threads were produced with anisotropic and isotropic topographies (Figure S1B, i-ii, Supporting Information). Specifically, upon electrospinning, the highest anisotropic degree was observed in A-Threads collected at higher speeds (v6, 1.09 cm s^{-1}) presenting diameters of 104.3 ± 3.1 µm, and microfiber widths of 1.3 ± 0.4 µm (Figure S1C-D, i, Supporting Information). Remarkably, the obtained fibers closely resembled the dimensions of the elementary unit of tendon tissue - primary collagen fibers[27]. Nonetheless, To replicate the fiber bundles macro-architecture of tendon fascicles, A-Threads/PL were twisted into yarns consisting of 12 threads covering the full-length scale units of tendon tissue [27b]. Isotropic fiber threads were also fabricated to replicate the randomly organized ECM of cancellous bone, specifically the fibrillar collagen network [28]. A peak absence in the orientation angle frequency of I-Threads confirmed the production of isotropic topography induced by the lowest collection speed (v1, 0.17 cm s^{-1}). Threads were produced with dimensions of 379.7 ± 70.3 µm and formed by fibers ranging with 1.2 ± 0.3 µm (Figure S1D, ii, Supporting Information), measurements falling within the dimensions of targeted trabecular network and mineralized collagen bundles[29].

Based on these results, the speed of 1.06 cm s^{-1} was selected for production of A-Threads whereas 0.17 cm s^{-1} was selected for production of I-Threads aiming at tendon and bone ECM structural replication, respectively.

2.2. Incorporation of PL within electrospun fiber cores

In an emulsion electrospinning process, emulsion droplets move perpendicularly from the surface to the center suffering an enrichment in the axial region, where droplets are stretched into an elliptical shape in the direction of the fiber trajectory, becoming entrapped inside electrospun fibers[16]. In this work, we explored this fabrication strategy to incorporate bioactive molecules present in PL within

fiber cores (**Figure 1A**, i). To start, droplets' diameter and dispersion of aqueous phase were two critical W/O emulsion parameters optimized for achieving a continuous spinning and efficient incorporation of PL within fibers[30]. Transmitted light microscope images revealed that homogenous emulsions could be obtained through the application of increasing ultrasonication amplitudes (**Figure 1B**, i). Specifically, among tested conditions, an amplitude of 50% for 2 minutes induced the formation of droplets with the smallest diameter (**Figure 1B**, i; 6.34 ± 3.39 µm) and lower polydispersion (**Figure 1B**, ii). Thus, the obtained emulsion can be classified as fine[30a] without major noticeable phase separation, suggesting that an amplitude of 50% for 2 minutes is well suited for the PL emulsions preparation.

Recently, emulsion centrifugal spinning has been applied for the incorporation platelet lyophilizes within microfibrous scaffolds[31]. Yet, the need for high amounts of surfactants to produce the spinning emulsions and its colloidal low stability are among the identified limitations of this strategy of fiber scaffolds production[31]. In the present work, PLs were incorporated in the aqueous phase of the W/O emulsions without requiring additional surfactants. This was observed in tests of emulsions stability, where no separation between the polymeric solution and aqueous phase was observed after leaving emulsion solutions to rest for 1 day (Figure S2, Supporting Information). This could be explained following the thermodynamic laws that all systems should be at their global minimum energy state, W/O dispersions rapidly separate into 2 phases to minimize the interfacial contact area and the free energy [32]. Separation or de-emulsification rate can be controlled by reducing the interfacial tension between the continuous phase and the dispersed droplets by adding an amphiphilic molecule, such as albumin, that acts as surfactant by adsorbing to and orienting itself at the interface in such a way that its nonpolar (hydrophobic) segment is partitioned into the polymeric phase of the solution and its hydrophilic part exposed to the aqueous phase, protecting more protein of interest[32-33]. So, the stability observed in prepared solutions might be explained by the high concentrations of albumin present in PL[20b].

The impact of emulsion quality on the entrapment of aqueous phase molecules on electrospun fibers was also assessed adding small amounts of fluorescent BSA-fluorescein to PL for visualization (**Figure 1C**). As shown by confocal imaging, fluorescent BSA-fluorescein were poorly dispersed within fibers when using emulsion solutions prepared using lower ultrasonication amplitudes (**Figure 1C**, i-

ii; 20% - 30%). On the other hand, as observed in **Figure 1C**, ii, well-dispersed incorporation was observed for the sonication at highest amplitude (50%, 2 minutes), resulting in bead-free and highly homogeneous nanofibers with PL cores. This results from the W/O emulsification process, where shell formation is associated with the evaporation of solvents in the hydrophobic polymeric solution (oil phase)[34] followed by a solidification process as result of vapor induce surface precipitation by the non-solvent atmospheric water and further contact with the liquid support bath[35]. Biomolecules present in the water phase are elongated and migrate to the center of the jet due to the viscosity gradient, instead of escaping onto fibers surface[34], enabling the formation of core-shell fibers with continuously disperse PL content.

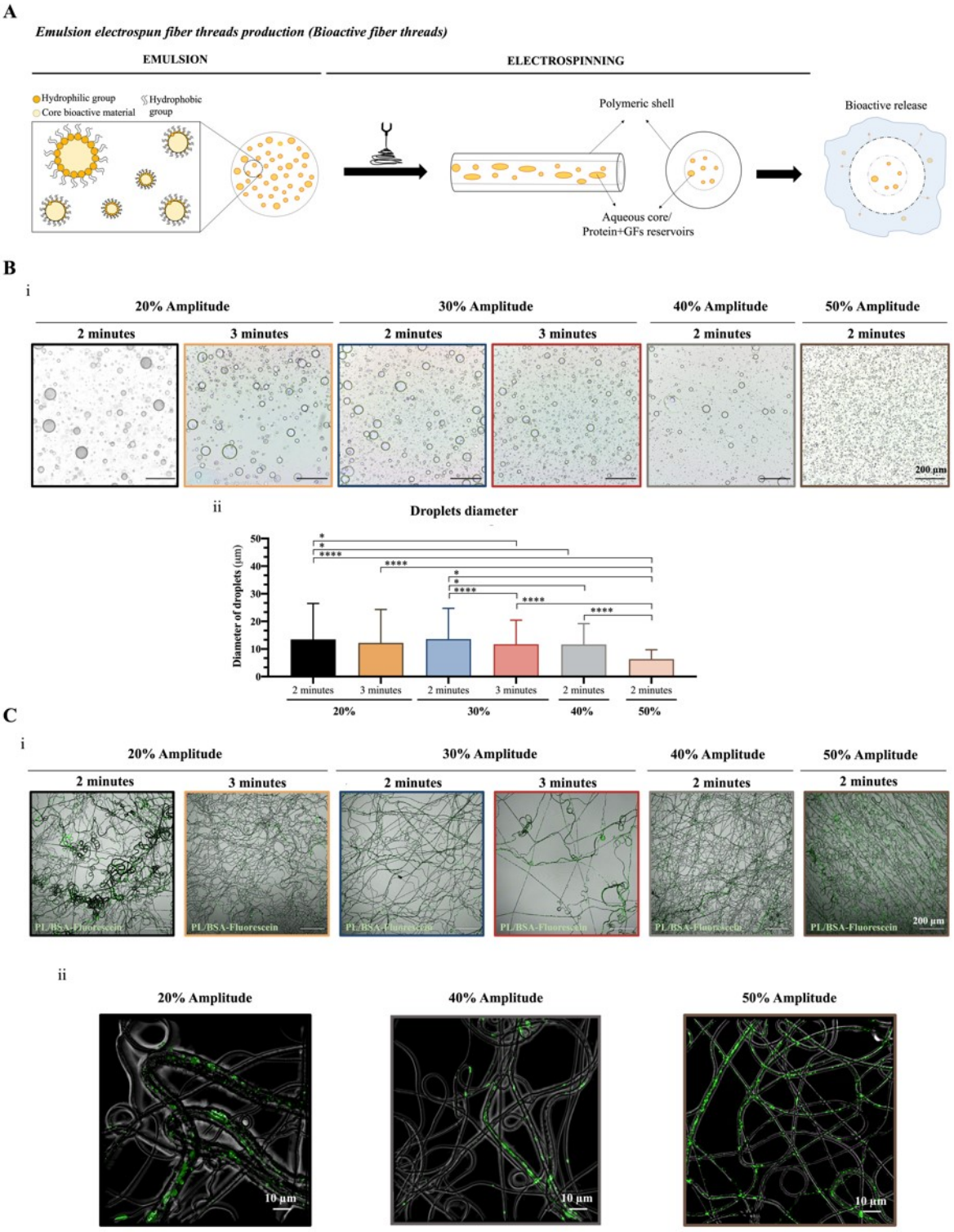

Figure 1. Emulsion solution parameters optimization and fibers production. (A) Schematics of emulsion electrospinning demonstrating the incorporation of bioactive molecules within electrospun fibers for a controlled local release. **(B)** Light reflected images of (i) emulsion droplets containing PLs and color dye after the application of increasing ultrasonication amplitudes: 20% and 30% for 2-3 minutes, and 40% and 50% for 2 minutes. Scale bars, 200 µm. Droplets average diameter (ii, *, p = 0.028; ****, $p < 0.0001$) evaluated for the different tested ultrasonication amplitudes. Error bars represent SD. **(C)** Confocal fluorescence microscopy images of emulsion electrospun fibers incorporating PL/BSA-fluorescein after (i) 20% and 30% for 2-3 minutes, and 40% and 50% for 2 minutes. (ii) Higher magnifications obtained of fibers obtained after emulsions preparation using 20%, 40% and 50% ultrasonication amplitudes for 2 minutes. Scale bars: 200 µm (i) and 10 µm (ii).

2.2.1. Chemical, morphological and mechanical assessment of PL-incorporated yarns and threads

After the production of fiber threads with anisotropic and isotropic topographies, the chemical composition of PCL and PLs in A-Yarns/PL and I-Threads/PL was assessed (**Figure 3A**, i-ii**)**. FTIR-spectra exhibited several PCL characteristic bands at 1239 (C-O-C, asymmetric stretching), 1292 (C-O and C-C stretching), 1653 (C=O stretching, amide I), 2931 (asymmetric stretching -CH2) and 2858 cm^{-1} (symmetric stretching -CH2)[7b]. The characteristic bands of PL around 3286 cm^{-1}, commonly amide A, attributed to the -NH group from PL proteins, and by a band around 1600-1690 cm^{-1} (amides I, C=O stretching)[36] confirmed its presence in A-Yarns/PL and I-Threads/PL (**Figure 2A**, ii).

Further, the morphology of produced A-Yarns/PL and I-Threads/PL was evaluated using SEM and micro-CT analysis. As depicted in **Figure 2B**, the topographical orientation of fiber threads in A-Yarns/PL was not affected by manufacturing process, as also confirmed by the directionality frequency graphs, where the presence of a sharp peak in the orientation angle frequency demonstrated a tendency of fiber threads alignment in a single direction (Figure S3A, I, Supporting Information). In contrast, a peak absence in I-Threads/PL demonstrated no preferential orientation as result of its random organization (Figure S2A, ii, Supporting Information). Moreover, **Figure 2B**, i-c shows the influence of PL incorporation in fibers and yarns/threads diameters. It was observed an overall decrease in fibers diameters to the range of 0.75 ± 0.19 µm and 0.91 ± 0.26 µm for A-Yarns/PL and I-Threads/PL, respectively, compared to A-Yarns and I-Threads (1.31 ± 0.29 µm; 1.18 ±

0.27 µm, respectively, **Figure 2C**, i-ii). This effect could derive from changes in the W/O emulsion solution properties (namely lower viscosity, surface tension and high conductivity) resulting from the addition of an aqueous phase[37]. Additionally, the porosity of manufactured A-Yarns/PL and I-Threads/PL was evaluated as this is one key parameter that favors cell infiltration, nutrient and oxygen diffusion and colonization[38]. A-Yarns/PL presented a full-length porosity of 20.56 ± 3.45% while in I-Threads/PL it fell around 19.51 ± 1.14% (**Figure 2B**, iii-iv). Furthermore, significantly larger pore sizes were observed in A-Yarns/PL and I-Threads/PL when compared to the respective plain controls (Figure S3A, iii-iv, b, Supporting Information). Nonetheless, even though not significantly, a higher interconnectivity was observed in A-Yarns/PL and I-Threads/PL compared with controls, demonstrating that PL incorporation affects the threads inner porosity, interconnectivity and pore size.

The impact of PL incorporation in the tensile mechanical properties of yarns and threads was also evaluated (**Figure 2C** and Figure S3B, i-ii, Supporting Information). No significant differences were observed between young's modulus and ultimate tensile strength of A-Yarn/PL (23.78 ± 2.5 MPa; i, UTS: 4.7 ± 0.6 MPa) and A-Yarn (24.1 ± 3.9 MPa; UTS: 3.6 ± 0.9 MPa; **Figure 2C**, i, b**,** Figure S3B, i, Supporting Information, respectively). The Young's modulus and ultimate tensile strength of A-Yarns/PL are within the lower range of native tendons tensile properties (20-1200 MPa and 5-100 MPa, respectively)[39]. I-Threads/PL (4.2 ± 1.4 MPa; UTS: 1.0 ± 0.2 MPa) and I-Threads (6.1 ± 1.5 MPa; UTS: 0.9 ± 0.2 MPa) also revealed similar mechanical performance when compared in between them (**Figure 2C**, ii, b, Figure S3B, ii, Supporting Information). Overall, incorporation of PLs was found to not affect the morphology and mechanical properties of A-Yarns/PL and I-Threads/PL compared with plain controls, which might be explained by the good dispersion of aqueous solution inside the fibers (Figure S4, Supporting Information), that could have filled possible structural defects that could affect the mechanical performance of tested specimens.

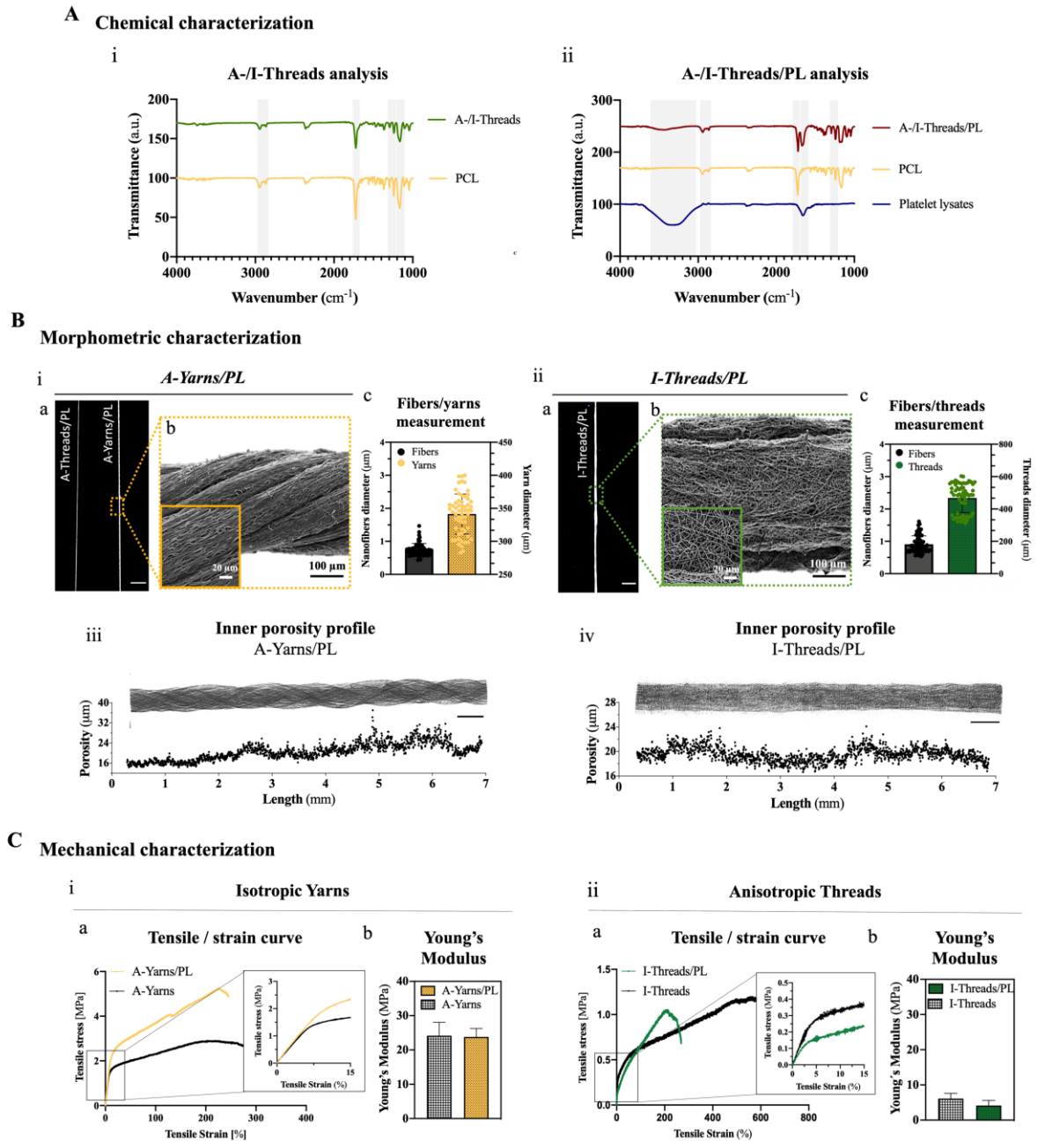

Figure 2. Chemical, morphological and mechanical characterization of A-Yarns/PL and I-Threads/PL. (A) FTIR spectra of neat PCL, PLs, and (i) A-/I-Threads and (ii) A-/I-Threads/PL with respective bands of interest identified. **(B)** Morphometric analysis of assembled (i) A-Yarns/PL and produced (ii) I-Threads/PL with (a) macro-scale images, (b) scanning-electron microscopy images, and (c) fiber and yarns/threads diameter measurements. Scale bars, 500 µm, 20 µm and 100 µm. Error bars represent SD (Fibers, n=60; Yarns/Threads, n=60). Microtomography (Micro-CT) 3D

reconstruction and respective longitudinal porosity analysis of (i) A-Yarns/PL and (ii) I-Threads/PL. Scale bars, 500 µm. Error bars represent SD. **(C)** Mechanical tensile testing of specimens with (a) representative tensile/strain curves and (b) calculated young's modulus for (i) A-Yarns vs A-Yarns/PL and (ii) I-Threads vs I-Threads/PL (n=5).

2.2.2. Nano-hydroxyapatite incorporation in isotropic threads

As a heterotypic tissue, the tendon-to-bone interface is constituted by distinctive ECMs with gradients of architecture and mineralization[25b]. The fibrocartilaginous insertion connects the highly aligned, fibrous tendon to the stiff and mineralized bone. Moreover, it is characterized by the presence of a non-mineralized and mineralized region, where normally an abrupt transition from cartilaginous to calcified fibrocartilage is observed. Thus, to enhance the potential of I-Threads/PL to induce osteogenic-like ECM deposition and mineralization, threads were modified with incorporation of nano-hydroxyapatite (nHAp) and thus closely resembling bone's nanocomposite nature, specifically the interconnected intrafibrillar and extrafibrillar minerals on the nanometer scale[40]. As reported in the literature, concentrations as low as 1% w/w of solid scaffold weight were shown to increase ALP activity and matrix mineralization in pre-osteoblast-like cells[41] and induce mesenchymal stem cells osteogenic commitment[42]. To boost the osteogenic potential of isotropic fiber threads without the need of pro-osteogenic factors and also a smooth fabrication of continuous I-Threads/PL incorporating these nanoparticles (I-Threads/PL@nHAp), a solid weight of 1% (w/w) was used during polymeric solution preparation. As observed in **figure 3A**-i, after alizarin red staining, I-Threads/PL@nHAp presented a good dispersion and incorporation of nHAp. Additionally, SEM imaging confirmed the absence of particles on the surface of the fibers, but an increased roughness was found when compared with I-Threads (**Figure 3A**-ii). Interestingly, the increase in fiber roughness has shown to have a positive effect on the osteogenic commitment of human mesenchymal stem cells, namely higher surface roughness induced higher expression of osteogenic genes such as osteopontin (OPN), bone morphogenetic protein 2 (BMP2), and runt-

related transcription factor 2 (RUNX2)[43]. Therefore, the higher I-Threads/PL@nHAp fiber roughness may contribute as an additional physical cue for osteogenic stem cells differentiation. Concerning the tensile mechanical performance of I-Threads/PL@nHAp, the incorporation of nHAp resulted in significantly lower Young's modulus (2.49 ± 1.50 MPa, **Figure 3B**, ii) and UTS (0.60 ± 0.17 MPa, **Figure 3B**, iii) compared to I-Threads@nHAp (5.72 ± 1.34 MPa and 1.51 ± 0.75 MPa). This could be explained by the effect of PL addition in I-threads/PL@nHap which resulted in a reduction of fibers stiffness. Overall, nHAp was successfully incorporated within I-Threads/PL@nHAp resulting in a topological alteration on fibers surface by increasing its roughness, important as an osteo-inductive cue for stem cells differentiation without the need of pro-osteogenic supplementation of medium.

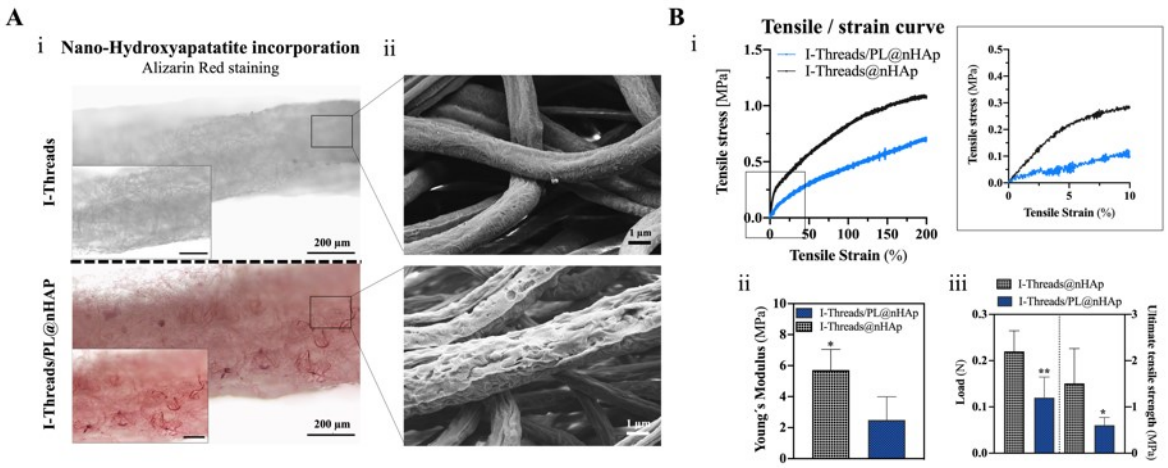

Figure 3. Morphometric and mechanical characterization of I-Threads and I-Threads/PL incorporated with nHAp. (A) Optical microscope images of (i) alizarin red staining of I-Threads (Top) and I-Threads/PL@nHAp (bottom). Scale bars, 200 µm. (ii) SEM images of fibers in both I-Threads (Top) and I-Threads/PL@nHAp (bottom). Scale bars, 1 µm. **(B)** Mechanical tensile testing of I-Threads @nHAp and I-Threads/PL@nHAp with (i) representative tensile/strain curves, (ii) calculated young's modulus and (iii) analysis of (*, p = 0.016) and tensile load and ultimate tensile (*, p = 0.031; **, p = 0.0077). Error bars represent SD (n=5).

2.3. A-Yarns/PL and I-Threads/PL as biological delivery systems

Human tissue's pH is tightly regulated in the living organism, ranging from 7.35 to 7.45[44]. After injury, pH-associated deviations occur under conditions in which oxygen cannot be properly transported, resulting in tissues damage[45]. Further, in wound healing, the tissues microenvironment pH value is suggested as a parameter for diagnostic purposes[46], and more recently, advances in the field of stimuli-responsive drug delivery used the pH as an endogenous trigger for programmed in situ drug release[47]. Therefore, defining and controlling the environmental tissues niche alterations is the key for a successful tissue regeneration. In this study, two different pH conditions (7.4 and 6.4) were used to simulate the physiological (healthy) and injured (inflammatory) states of tendon-to-bone tissue interface aiming at understanding their impact on the release kinetics of PL molecules from A-Yarns/PL and I-Threads/PL under the different conditions of the tissue healing process (**Figure 4**).

First, the cumulative release of total proteins was evaluated up to 31 days. Since proteins were in the core of fibers, a sustained and slow released is observed for both A-Yarns/PL and I-Threads/PL under physiological and inflammatory conditions (**Figure 4A**).

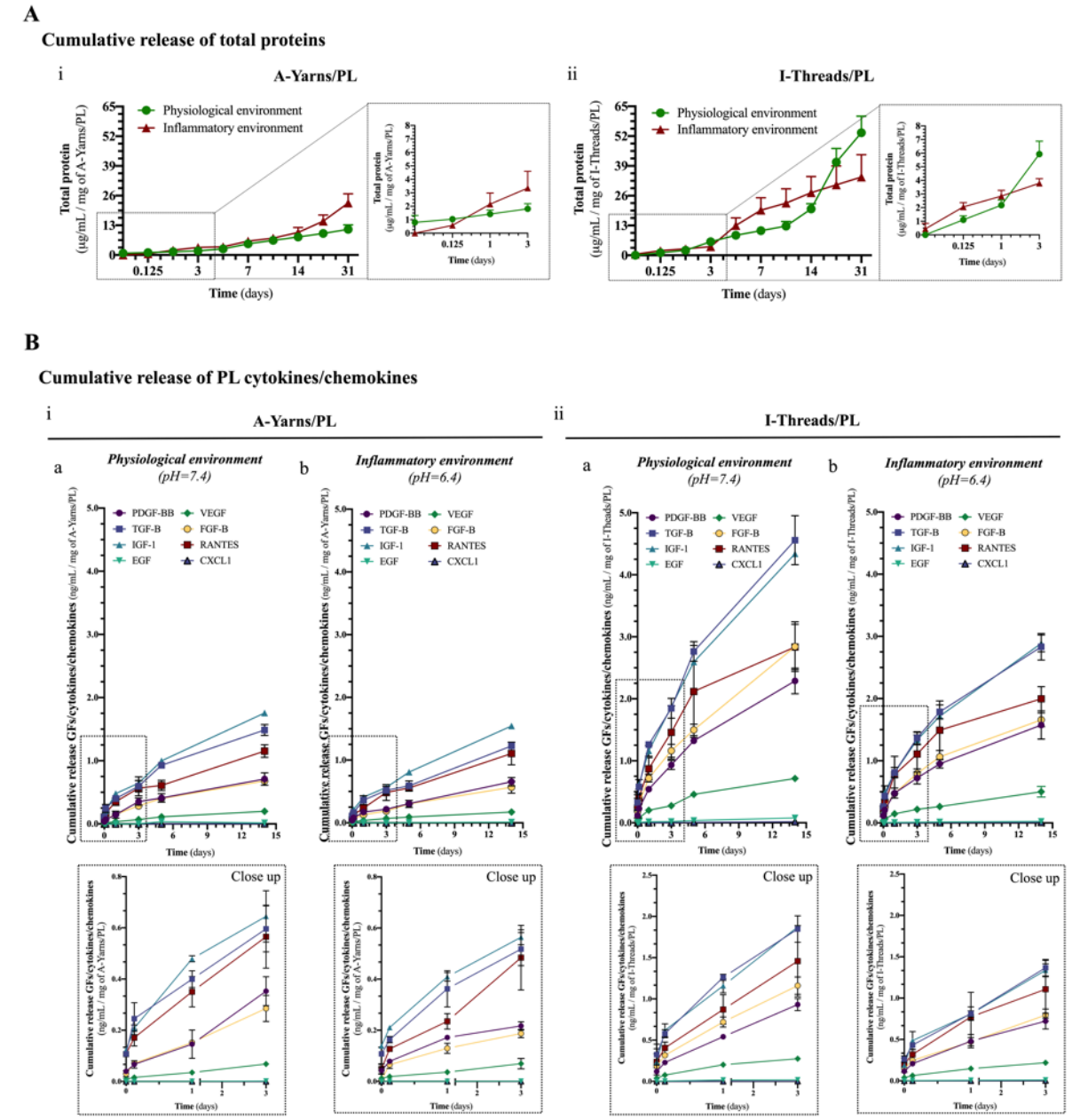

Figure 4. Profile release of total proteins and PL growth factors, chemokines and cytokines in physiological and inflammatory environments. (A) Cumulative total protein release from (i) A-Yarns/PL and (ii) I-Threads/PL after contact with physiological and inflammatory environments for 31 days. Error bars represent standard error mean (SEM) (n=5). **(C)** Cumulative release of PL growth factors (GFs), cytokines and chemokines, namely PDGF-ß, TGF- ß, IGF-1, EGF, VEGF, FGF, ß, RANTES

and CXCL1, quantified by ELISA in both (i) A-Yarns/PL and (ii) I-Threads/PL in both (a) physiological and (b) inflammatory settings for 14 days. Error bars represent SD (n=3).

Interestingly, higher amounts of proteins were released under inflammatory pH comparably to physiological pH, which might be associated with the faster polymer degradation, namely accelerated hydrolysis under acidic conditions, and solubilization of easily accessible proteins[48]. Additionally, higher release was observed for I-Threads/PL comparably with A-Yarns/PL (**Figure 4B**, i-ii), which could be related with threads microstructural differences, namely threads dimensions, fibers number, and porosity. This behavior could also be observed in terms of water uptake/weight loss kinetics (Figure S5B, Supporting Information), where the highest uptake was observed in threads independently of the incorporation of PL. Nevertheless, it should be noted that these mechanism can differ in an *in vivo* setting, where the presence of macrophages or even metalloproteinases at a wound site can contribute to an accelerated polymer degradation[49].

The release of the PL components with known relevant roles on tendon-to-bone healing [50] namely, platelet-derived growth factor-BB subunit (PDGF-BB), transforming growth factor-ß (TGF-ß), insulin growth factor-1 (IGF-1), epidermal growth factor (EGF), vascular endothelia growth factor (VEGF), fibroblast growth factor-ß (FGF-ß), RANTES and CXCL1 were similarly evaluated up to 14 days. As depicted in Figure 4B and Table 1, I-Threads/PL released higher concentrations of GFs, cytokines and chemokines when compared with A-Yarns/PL at both testing settings. This difference might be related with a higher accessibility of incubation solution to the inner microfibers in the I-Threads than in the more compact uniaxially aligned A-Yarns.

When assessing the release profile of both tested yarns and threads after 14 days, higher amounts of PDGF, IGF-1, TGF-ß, FGF- ß and RANTES, important factors for mesenchymal stem cells osteogenic induction[51] were observed for I-Threads/PL, whilst TGF-ß, IGF-1 and RANTES, described together as inducers of tenogenic matrix synthesis and/or cell proliferation [52], showed higher release in A-Yarns/PL, at both physiological and inflammatory settings (**Figure 4B**, **Table 1**). On the other hand, the cumulative released concentration of some GFs such as PDGF-BB after 14 days was found to be within a range (~0.2 to 10.0 ng/mL; **Table 1**) described to induce cells proliferation and

differentiation in *in vitro* cell cultures[53]. However, even though the release of biomolecules is within the pretended concentrations, when scaffolds are seeded with cells, the presentation of PL biomolecules in close proximity to the cell receptor at the surface of the fibers is a much more biomimetic way of presenting PL biomolecules than adding it to culture media, as commonly performed in vitro culture procedures, potentiating their effects and prevent a fast proteolytic degradation[54].

Table 1. Average cumulative release of GFs, cytokines and chemokines of A-Yarns/PL and I-Threads/PL after 14 days under physiological and inflammatory settings.

Average cumulative release (ng/ml/mg sample)		*Growth Factors/cytokines/chemokines*							
		PDGF-BB	**TGF-B**	**IGF-1**	**EGF**	**VEGF**	**FGF-B**	**RANTES**	**CCLX1**
A-Yarns/PL	Physio.	0.71±0.10	1.49±0.09	1.76±0.05	0.016±0.0002	0.20±0.03	0.68±0.05	1.15±0.10	0.004±0.0001
	Inflam.	0.66±0.07	1.23±0.01	1.55±0.01	0.012±0.001	0.17±0.02	0.57±0.09	1.11±0.18	0.001±0.0001
I-Threads/PL	Physio.	2.29±0.21	4.56±0.40	4.34±0.01	0.08±0.02	0.71±0.03	2.84±0.40	2.84±0.37	0.02±0.003
	Inflam.	1.57±0.23	2.83±0.21	2.89±0.14	0.024±0.004	0.50±0.09	1.66±0.11	1.99±0.20	0.010±0.0001

2.4. Biological performance of biofunctional yarns and threads

To evaluate the effects stemming from the synergy between the biological activity of PLs components and topographical cues of anisotropic yarns and isotropic threads, A-Yarns/PL and I-Threads/PL were seeded with hASCs, an easily available stem-cell source for tendon- and bone-tissue engineering[55], and compared with the plain controls. Figure 5A reveals a significant increase in hASCs proliferation after 10 and 15 days of culture in contact with A-Yarns/PL and I-Threads/PL compared to A-Yarns and I-Threads, respectively, reflecting the effects of PL incorporation on the scaffold's a biological activity. Interestingly, the intracellular alkaline phosphatase (ALP) activity, an important indicator of osteogenic commitment[56], of hASCs seeded in I-Threads/PL was 5.1-, 1.7- and 1.4-fold increased at days 5, 10, and 15 in comparison with the values found in I-Threads (**Figure 5B**), demonstrating the potential of bioactive threads to induce an osteogenic response in stem cells. In the case of hASCs seeded A-Yarns/PL, ALP activity is reduced during culture time.

The expression of scleraxis (SCX), an important transcription factor in tendon tissue formation and expressed during tendon development[57], was assessed in both hASCs-seeded A-Yarns/PL, I-Threads/PL and respective plain controls (**Figure 5C**, i-ii). A-Yarns/PL showed a significantly higher expression of SCX at 5 and 10 days compared to A-Yarns. Remarkably, SCX expression was accompanied by a translocation into cells' nuclei (Figure 5C, i, c-d), demonstrating an activation of this transcription factor, and resultant commitment of stem cells towards the tenogenic lineage[58]. Nevertheless, even though a temporal increase in SCX expression was observed in I-Threads/PL, nuclei translocation did not occur (**Figure 5C**, ii, c-d). Therefore, the conjugation of biological factors release and anisotropic orientation of produced A-Yarns/PL was found to induce a tenogenic response in hASCs. In Figure 5D, expression of collagen type III (COL3) was evaluated in hASCs seeded onto A-Yarns/PL, I-Threads/PL and respective plain controls, due to reported evidence of the key role of this protein in bone ECM during tissue development and healing[59] and its relation with states of tendon degeneration and pathophysiology[60]. During culture time, no differences were observed in the expression of COL3 between A-Yarns/PL and A-Yarns (**Figure 5D**, i, a-b). In contrast, at both 5 and 10 days of culture, I-Threads/PL induced a significant higher deposition of COL3

compared with I-Threads (**Figure 5D**, i, a-b), demonstrating the potential of these fibers to sustain the deposition of an osteogenic-like ECM. Nevertheless, the pro-osteogenic potential of fiber threads incorporated with nHAp was similarly assessed, envisioning its use as reliable biomaterials for osteo-commitment of stem cells. The biological performance of hASCs in terms of cell proliferation and ALP activity was also assessed in I-Threads/PL@nHAp over a culture period of 15 days in basal medium conditions and compared with respective controls (I-Threads@nHAp) (**Figure 5E**). As expected, I-Threads/PL@nHAp induced a significantly higher proliferation (1.2- and 3.1-fold increase at days 5 and 10, respectively), and enhanced ALP activity compared to I-Threads@nHAp. Additionally, and given the importance of ECM mineralization on the determination of cells commitment towards the osteogenic lineage[61], alizarin red assay was performed at both 5 and 15 days of culture in several groups, namely I-Threads, I-Threads@nHAp, I-Threads/PL and I-Threads/PL@nHAp (**Figure 5F**, i-ii). Optical images of stained threads confirmed an absence of matrix mineralization in I-Threads in both 5 and 15 days. In contrast, even though some mineralization was found in I-Threads@nHAp and I-Threads/PL, an extensive staining was observed in I-Threads/PL@nHAp (**Figure 5F**, i). This visual information was afterward confirmed by alizarin red quantification (Figure 5F, ii), where significantly higher AZ dye concentration was obtained for I-Threads/PL@nHAp, at both 5 and 10 days of culture under basal conditions, compared with the other tested threads formulations. Overall, the synergistic effect between the mineral component, fibers topography and PLs biological factors enabled the induction of hASCs towards osteogenic lineage without the need of an external biochemical supplementation.

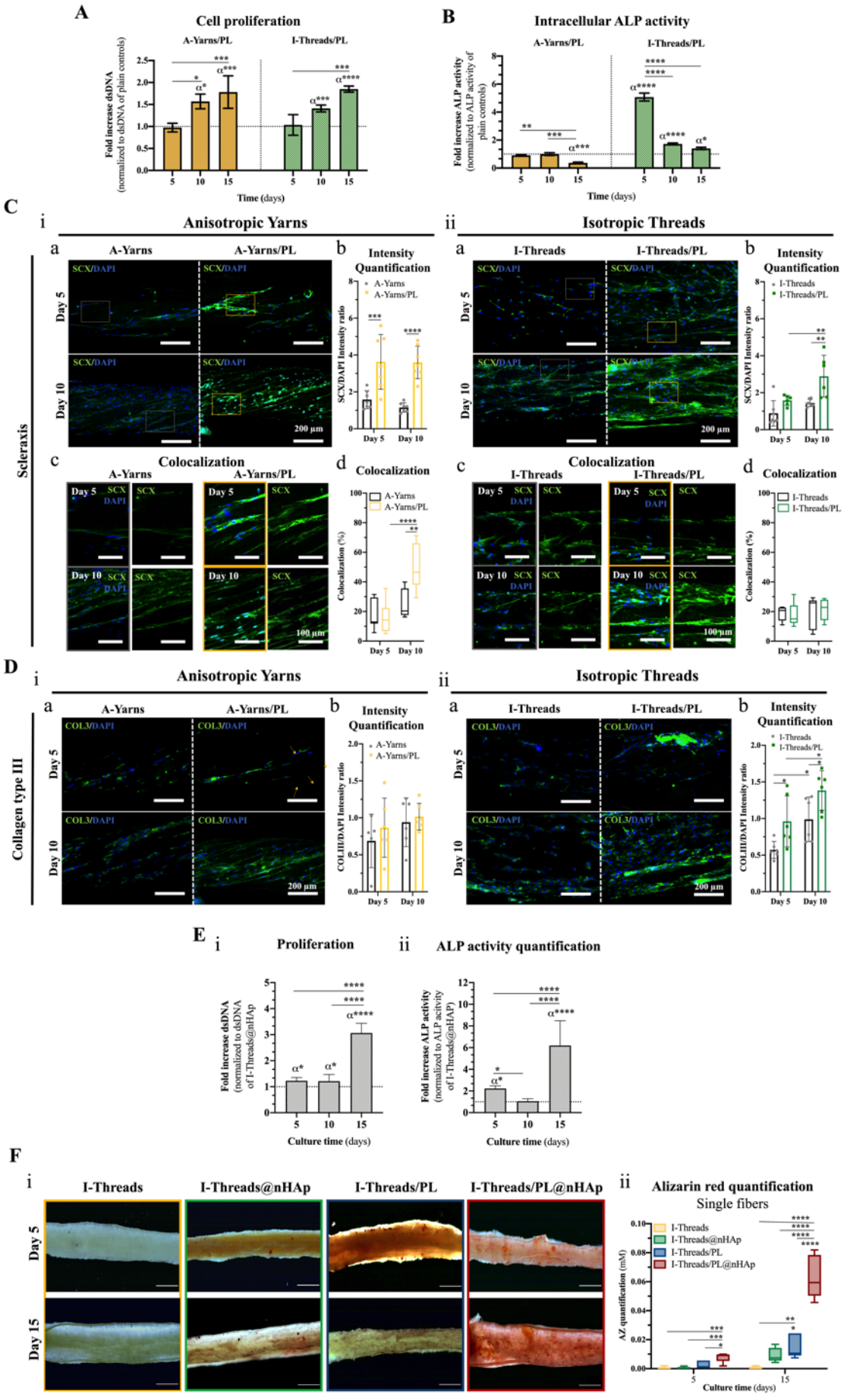

Figure 5. Cell proliferation, ALP activity, protein expression and matrix mineralization of hASCs seeded A-Yarns/PL, I-Threads/PL and I-Threads/PL@nHAp. (A) Fold increase in hASCs proliferation in A-Yarns/PL (*, p = 0.020; ***, p = 0.0004) and I-Threads/PL (***, p = 0.0005; ****, p < 0.0001) compared with A-Yarns and I-Threads, respectively, at 5, 10 and 15 days of culture. Error bars represent SEM (n=9) **(B)** Fold increase in intracellular ALP activity in A-Yarns/PL (**, p = 0.0019; ***, p = 0.0003) and I-Threads/PL (*, p = 0.028; ****, p < 0.0001) compared with A-Yarns and I-Threads at 5, 10 and 15 days of culture. Error bars represent SEM (n=9). **(C)** Immunofluorescence imaging of (a) scleraxis (SCX) and respective (b) intensity ratio in A-Yarns vs A-Yarns/PL (***, p = 0.0006; ****, p < 0.0001) and I-Threads vs I-Threads/PL (**, p = 0.0053). (c) Nuclei colocalization of SCX (green channel) after 5 and 10 days of culture in both (i) A-Yarns vs A-Yarns/PL and (ii) I-Threads vs I-Threads/PL and respective (d) colocalization percentage (**, p = 0.0016; ****, p < 0.0001). Scale bars, 200 µm and 100 µm. Error bars represent SD (n=7). **(D)** Immunolabeling of matrix protein, (a) collagen type III (COL3) after 5 and 10 days of culture in (i) A-Yarns vs A-Yarns/PL and (ii) I-Threads vs I-Threads/PL and respective (b) intensity ratio (*, p = 0.045). Scale bars, 200 µm. Error bars represent SD (n=5). **(E)** Cell's proliferation (i, *, p = 0.039; ****, p < 0.0001) and intracellular ALP activity (ii, *, p = 0.031; ****, p < 0.0001) of seeded hASCs up 15 days of culture in I-Threads/PL@nHAp. Fold increase obtained through normalization against the values obtained for I-Threads@nHAp. Bars represent SD (n=9). Statistical differences between I-Threads/PL@nHAp and I-Threads@nHAp are shown as α. **(G)** Optical microscopy images of (i) alizarin red staining after 5 and 15 days of culture of hASCs seeded I-Threads, I-Threads@nHAp, I-Threads/PL and I-Threads/PL@nHAp. Scale bars, 500 µm. (ii) Alizarin red quantification performed at 5 and 15 days of culture for the previously stained isotropic threads (*, p = 0.015; **, p = 0.0046; ***, p = 0.0004; ****, p < 0.0001). Bars represent the maximum and minimum values (n=5).

2.5. 3D functionally graded scaffolds: textile assembling technique

Over the past year, various biomaterials fabrication strategies have been devised for the replication of the hierarchical organization of soft-to-hard tissue interfaces. Particular attention has been given to textile technologies for the fabrication of mechanically and biologically competent 3D scaffolds. Knitting, weaving and braiding have been used to create constructs closely reaching the properties of different soft-to-hard tissues, while conserving key features of their single units in an assembled hierarchical construct[62]. Still, developed technologies have shown limited potential to provide crucial bioactive signals for these complex microenvironments in a precise and controllable manner, often not reaching the aimed biological response. As observed in **Figure 6A**, by simply interlocking

anisotropic yarns and isotropic threads, we developed continuous, easily handled and highly reproducible **(**Table S1, Supporting Information) gradient scaffolds with three distinct zones: a tendon insertion, an interface resultant of the conjugation of yarns and threads, and a bony part (**Figure 7A**, iv), within the micro-scale range of tendon-to-bone tissue interface[63]. Micro-CT analysis allowed to confirm the spatial transition of the scaffold's microstructural cues, as well as its mineral content (**Figure 6B** and Figure S6, Supporting Information). Further, the presence of nHAp within threads was confirmed by fluorescence microscopy after alizarin red staining (**Figure 6D**, i-ii).

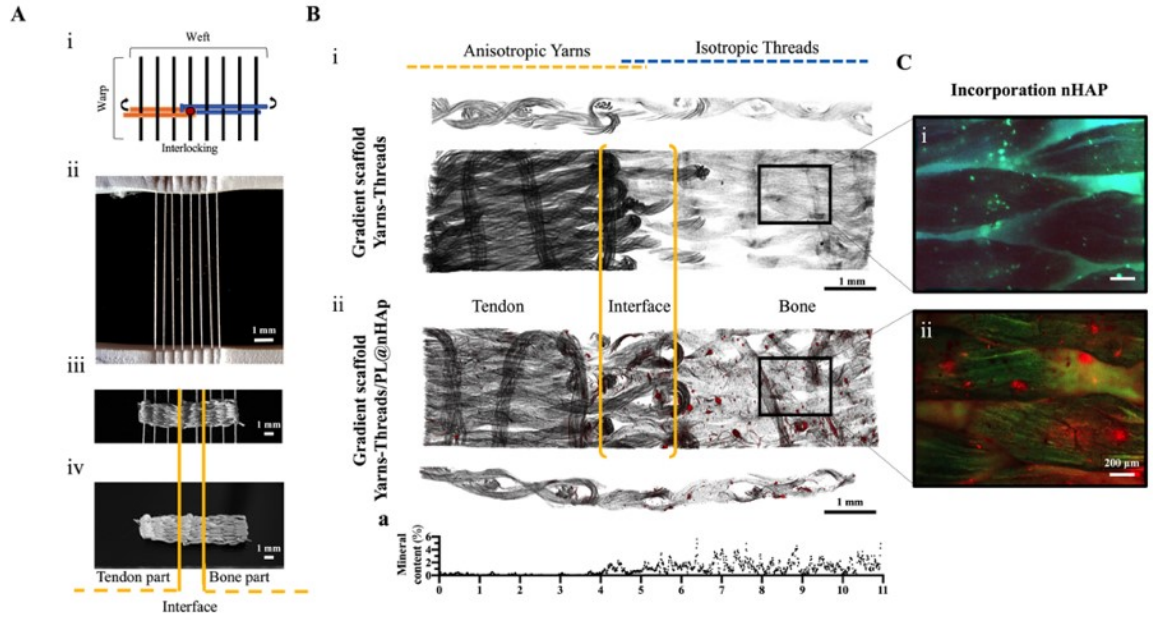

Figure 6. Production and morphometric analysis of developed 3D gradient scaffolds. (A) Schematics of textile assembling taking advantage of (i) weaving technique and (ii) used platform for the continuous weft of anisotropic yarns and isotropic threads, resulting in the fabrication of continuous gradient scaffold (iii-iv). Scale bars, 1 mm. **(B)** Micro-CT scans of full-length and transversal cuts of (i) gradient scaffolds produced using A-Yarns and I-Threads (Scaffold Yarns-Threads) and (ii) A-Yarns/PL and I-Threads/PL@nHAp (Scaffold Yarns-Threads/PL@nHAp). Hydroxyapatite particles are represented in red. Scale bar, 1 mm. (a) Graphical demonstration of the mineral content of across produced Yarns-Threads/PL@nHAp scaffold. **(C)** Immunofluorescence imaging of alizarin red-stained (i) Yarns-Threads and (ii) Yarns-Threads/PL@nHAp scaffolds. Particles are identified in red. Scale bar, 200 µm.

2.5.1. Biological performance of 3D gradient scaffolds: expression of tendon, interface and bone-related markers

The evaluation of biological performance of the developed gradient scaffolds, focused on assessing the effect of microstructural, topographical and compositional on the localized expression of specific tissue-related markers by hASCs without requiring additional biochemical supplementation. To investigate the capacity of produced functionally graded scaffolds to induce the deposition of characteristic collagenous matrix commonly found in the interface[1a], the regional deposition of collagen and non-collagenous proteins in the construct was assessed (Figure S7A, Supporting Information). Interestingly, quantitative data demonstrated higher collagen accumulation in the tendon- and bony-parts of the Yarns-Threads/PL@nHAp in comparison with plain controls and Yarns-Threads@nHAp (Figure S6A, ii, a), even though an even deposition of collagenous matrix was quantified throughout the scaffold. Remarkably, when assessing non-collagenous proteins, the highest accumulation occurred in the tendinous sections of Yarns-Threads/PL@nHAp compared with plain controls and Yarns-Threads@nHAp, and even the bony section of the scaffold (Figure S7A, ii, a), which might be associated with stimulatory effect of PL within scaffolds to sustain a higher deposition of tenogenic noncollagenous matrix components, namely proteoglycans, glycoproteins, and glycoconjugates, that play an important role within the tissue[64]. Additionally, the expression of interface-related markers, SRY-Box Transcription Factor 9 (SOX9) and type II collagen (COL2) was studied in fabricated scaffolds after 21 days of culture under basal conditions (**Figure 7**). When assessing both proteins expression across scaffolds full-length, hASCs-seeded Yarns-Threads@nHAp and Yarns-Threads show a dispersed and non-regional specific expression (**Figure 7**, i-ii). In contrast, zonal specific expression was observed for Yarns-Threads/PL@nHAp, namely through a higher COL2 deposition observed in both tendon and interface parts (non-mineralized fibrocartilaginous section) of the constructs (**Figure 7**, iii, red), and SOX9 expression mainly localized in the interface (mineralized fibrocartilaginous section) and bony-sections (**Figure 7**, iii, green). Furthermore, to confirm the biomineralization potential of produced scaffolds, alizarin red staining was performed (Figure S7B, Supporting Information). As expected, matrix mineralization was concentrated in the interface-bone sections of Yarns-Threads/PL@nHAp and Yarns-Threads@nHAp scaffolds (Figure S7B,

ii, Supporting Information), demonstrating a possible commitment of hASCs into the osteogenic lineage in that region associated with the presence of nHAp.

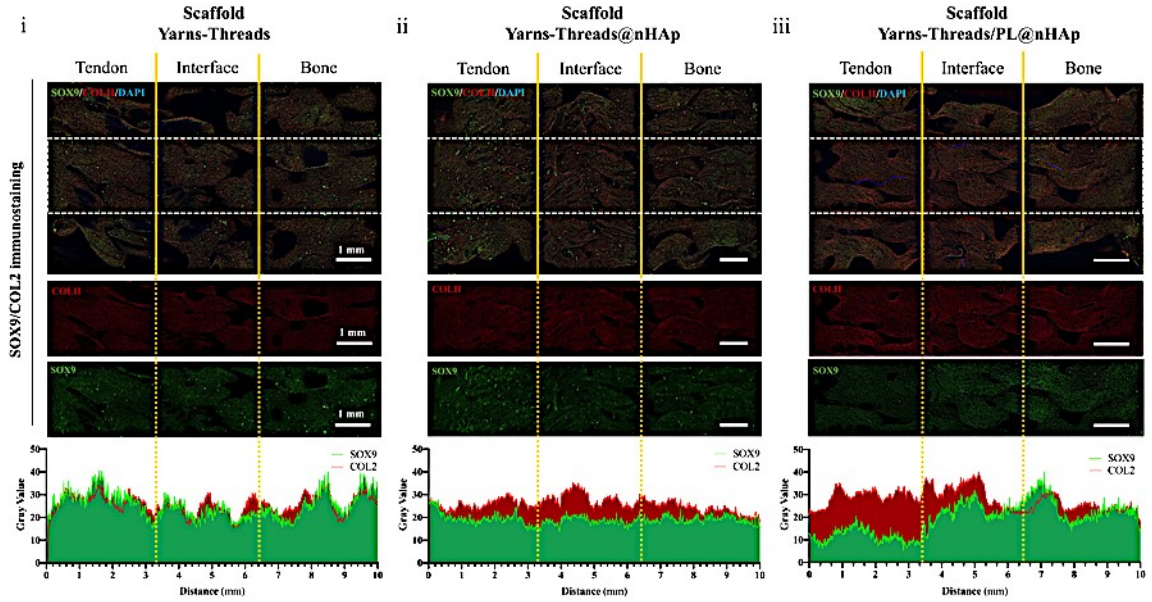

Figure 7. Expression of interface-relevant markers in hASCs-seeded 3D graded scaffolds. Immunostaining of interface-related markers (collagen type II, COLII; SRY-Box transcription factor SOX9, SOX9) after 21 days of culture in (i) Yarns-Threads, (ii) Yarns-Threads@nHAp and (iii) Yarn-Threads/PL@nHAp scaffolds seeded with hASCs. Scale bar, 500 µm. The respective gray value of immunolabeling for each marker was determined across scaffolds length and divided according to the different parts (dotted lines).

Overall, these results suggest that the 3D hierarchical architecture, topography and composition of the proposed functionally graded scaffolds can induce the deposition of a COL2 rich matrix in the non-mineralized fibrocartilaginous section of the interface, the osteochondrogenic commitment of stem cells at the mineralized fibrocartilaginous section, while inducing matrix mineralization at interface-bony-part, thus promoting the deposition of ECM resembling that of native tendon-to-bone interface. It should be noted that these results demonstrate the feasibility of constructs to be

used as possible replacements of injured tendon-to-bone interface tissues as these are able to replicate the tendon-to-bone microstructure while providing the necessary cues for spatial-specific stem cell commitment. Nevertheless, *in vivo* studies using clinically relevant models of tendon injury will need to be conducted to quantitatively evaluate their regenerative performance.

3. Conclusion

In this work, we developed functionally graded 3D scaffolds containing bioactive factors for heterotypic tissues replacement. This was achieved using emulsion electrospinning for the incorporation of PL within isotropic and anisotropic-tissue mimetic structures, namely bone and tendon, respectively. Additionally, nHAp was incorporated in threads to closely replicate the bone mineral content. PL-incorporated yarns and threads demonstrated to support a sustained release of biological factors when maintained in physiological (neutral pH) and inflammatory (acidic pH) settings without losing their bioactivity. In fact, this was confirmed in biological studies with hASCs, where seeded A-Yarns/PL and I-Threads/PL@nHAp revealed not only to be able to support cell proliferation but also to favor the expression of tenogenic-markers or to induce an osteogenic-like phenotype, respectively, without the need of external biochemical supplementation. Moreover, the combination of emulsion electrospinning and textile technologies, enabled the generation of 3D functional scaffolds with gradients in composition and topography, important to tailor hASCs commitment into chondrogenic and osteochondrogenic lineages in the interfacial space of constructs. Altogether, our results represent a promising strategy for the fabrication of reproducible 3D functionally graded scaffolds for complex hierarchical tissues regeneration, namely the tendon-to-bone interface.

4. Experimental Section

Preparation of human platelet lysates: Platelet concentrates (PC) from healthy human blood donors were used to obtain platelet lysates (PLs). The PC samples were provided by Instituto Português do Sangue (IPS; Porto, Portugal), under a previously established cooperation protocol. All the products were biologically qualified according to Portuguese legislation, undergoing standard testing for blood transfusion acceptance. PL was obtained according to optimized protocols [65]. Briefly, PC with a platelet count of 1 million platelets/µL were used. To reduce batch-to-batch variability, a pool of platelet concentrates from 10-12 donors was used and subjected to three different freeze/thaw cycles using liquid nitrogen and a water bath, respectively, to promote platelet lysis and protein release. Platelet debris was removed after centrifugation at 1400g for 10 minutes at 4 °C and supernatants were stored at -80 °C. Prior to use, platelet lysates (PLs) samples were allowed to thaw at room temperature (RT), filtered using a pore size of 0.22 µm and kept on ice until solution preparation.

Optimization of water-in-oil emulsions: A polymeric solution (oil phase) of 17% (w/v) polycaprolactone (PCL, average Mn = 80 000, Merck, Germany) was prepared by dissolving the polymer in a mixture of chloroform /DMF (7:3, v/v; Merck, Germany) overnight at RT. Afterward, water-in-oil (W/O) emulsions were prepared by the addition of a mixture of blue food coloring and MilliQ water to PLs (1:1, v/v). The obtained solution was sonicated using an ultra-sonicator probe (Sonics&Materials, INC., VCX-130PB-220, EUA) for 2 min at 20, 30, 40 and 50% amplitude and 3 min at 20 and 30% amplitude. For an initial characterization prior to electrospinning, few drops w/o emulsions were mounted on a glass slide and observed under a reflected light microscope (Microscope Leica DM750, Germany). Images of emulsion droplets were acquired and analyzed for average diameter and dispersion. To study emulsions stability and phase separation, all solutions were left at rest for 24h inside the containers (Supplementary information, Figure S1). For the analysis of PL distribution after electrospinning, w/o emulsions were prepared containing FITC-BSA (Thermofisher, EUA; 5 mg/mL in MilliQ water) and PLs (1:1 ratio, v/v) in the aqueous phase. Afterward, using a previously optimized electrospinning setup [10b], emulsions were electrospun and a thin layer of fibers collected on a glass slide allowed to dry overnight at RT, and observed under confocal laser scanning microscopy (Leica TCS SP8, Microsystems, Wetzlar, Germany) to visualize the

presence and distribution of molecules within the electrospun fibers. form the acquired Z-stack images for each tested solution.

Production of electrospun and emulsion fiber threads with anisotropic and isotropic topographies: Water-in-oil (W/O) emulsions with PLs were prepared on the same day of electrospinning. Briefly, for the aqueous phase preparation, filtered PLs and MilliQ were mixed in a ratio of 1:1 (v/v), and a final volume of 200 µL dropped-wise to 1 mL of polymeric solution (oil phase, 17% PCL solution) under constant agitation. Afterward, using previously optimized conditions, the obtained solution was ultrasonicated on ice for 2 minutes at 50% amplitude. Within a period of 1 – 2 h, the acquired emulsion solutions were used for electrospinning. Continuous electrospun fiber threads with and without PLs were produced using a previously optimized electrospinning system developed by our group [10b] with some modifications. Briefly, pure polymeric or emulsion solutions contained in a syringe with a 21G needle were electrospun at a constant flow rate of 1.00 mL/h and a voltage of 8-12 KV to a grounded liquid support bath of water/ethanol (8:2, v/v), and continuously pulled by a winding collector placed at defined distances. To produce anisotropic fiber threads, the vertical distance (d_{Bath}, **Figure S1A**) from the needle to the support liquid bath was set at 16 cm, and the horizontal distance ($d_{Collector}$) to the collector was set at 20 cm. To produce isotropic fiber threads, the vertical and horizontal distances were set at 13 and 13 cm, respectively. Electrospun fiber threads were collected at RT (23±2 ºC) and humidity ranging from 45% to 50%. Several collection speeds were tested (v1, 0.14 cm s^{-1}; v2, 0.34 cm s^{-1}; v3, 0.54 cm s^{-1}; v4, 0.68 cm s^{-1}; v5, 0.82 cm $s^{-1}$and v6, 1.09 cm s^{-1}). Optimal collection speed conditions were set at 0.14 (v1) and 1.09 cm/s (v6) to produce anisotropic and isotropic threads, respectively. All fibers were left inside a desiccator switched on with a vacuum pump overnight to eliminate possible solvent from the production process. Produced anisotropic and isotropic fiber threads without PLs were thereafter called as A-Threads and I-Threads, respectively, while anisotropic and isotropic emulsion electrospun fiber threads containing PLs were denominated as A-Threads/PL and I-Threads/PL respectively. Concerning the fabrication of yarns, 12 anisotropically aligned fiber threads were grouped together and twisted at 4 turns cm^{-1}, and produced yarns without and with PLs were thereafter denominated as A-Yarns and A-Yarns/PL, respectively.

Incorporation of nHAp in isotropic threads: To replicate the organic phase composition of bone tissue as accurately as possible, I-Threads and I-Threads/PL were incorporated with nano-hydroxyapatite (nHAP, nanopowder, <200 nm particle size (BET), ≥97%, synthetic, Merck, Germany) particles. Briefly, nHAp was added to a PCL solution (17% w/v), representing 1% w/w of PCL. The obtained mixture was stirred at 150 rpm for 1-3 hours, at room temperature, and sonicated for 2 minutes until all the nHAP powder was dispersed. For emulsion preparation, the aqueous phase (PL/MilliQ, 1:1, v/v) was added to the obtained dispersion and ultrasonicated for 2 minutes at 50% amplitude. Right afterward, the obtained solutions were transferred into a syringe fitted with a 21G needle and electrospun at a constant flow rate of 1.00 mL h^{-1} and a voltage of 8-9 kV was applied during the process. Vertical and horizontal distance to the bath of 12 and 13 cm, respectively, and produced electrospun threads were collected at RT (25 ± 2ºC) and humidity ranging from 45% to 50%. Incorporated isotropic fiber threads without and with PLs were thereafter called as I-Threads@nHAp and I-Threads/PL@nHAp, respectively.

Textile assembling of 3D gradient scaffolds for tendon-to-bone hierarchical replication: To fabricate a 3D construct, weaving textile technique was applied to assemble the fibrous structures following a previously reported process [10b] with some adaptations. A handmade platform was produced, where 8 cotton threads were placed side by side with a distance of 0.5 cm. Anisotropic yarns and isotropic threads were sequentially used as warp/weft threads. This sequence was adjusted during the fabrication of scaffolds. In the middle, threads were interlocked, creating a continuous gradient of threads topography and composition. As a final step, respective threads were passed in between warp/weft threads and in the middle, to maintain the structural integrity of the scaffold. Three different types of constructs with dimensions between 10.69 ± 0.78 and 11.39 ± 2.13 were produced: 1) Yarns-Threads (plain control); 2) Yarns-Threads@nHAp; 3) Yarns-Threads/PL@nHAp.

Scanning electron microscopy (SEM) analysis and directionality analysis: The morphology of produced yarns and threads were analyzed by scanning electron microscope (SEM, MP1000001280128, JSM-6010 LV, JEOL). Samples were coated with 2 nm of platinum (Cressigton) before analysis. For I-Threads/PL@nHAp, samples were coated with 2 nm of gold (Cressigton) and analyzed by High-Resolution Field Emission Scanning Electron Microscope with Focused Ion Beam

(FIB – SEM). Concerning the degree of topographical alignment, this parameter was determined through directionality analysis applying the Fourier components method using the FIJI software (version 2.0.0-rc-69/1.52p). For this purpose, scanning electron images were converted to 8-bit images and cropped into three different images. The radial intensities were calculated, and the orientation map was also obtained.

Micro-CT analysis: Plain and PL-incorporated yarns and threads microstructure was evaluated by X-rays micro-computed tomography (micro-CT) using a high-resolution system Skyscan scanner (Skyscan 1272; Bruker, Billerica, MA, USA). The acquisition of X-ray images was performed with a pixel size of 4.25 µm, a rotation step of 0.2° over 360°, and a smoothing averaging of every two images, using the SkyScan acquisition software version 1.1.3. The X-ray source was fixed at 35 kV and 181 µA of voltage and current, respectively. Following the acquisition, gray-scale images were reconstructed using the NRecon software (version 1.7.1.0). Then, when needed, the samples were vertically aligned for the cross-sectional analysis of the fibers using the DataViewer software (version 1.5.3.6). Qualitative visualization of the 3D morphology was performed using CT-Vox software (version 3.3.0). Quantitative analysis was performed after converting the regions of interest into binary images by a dynamic threshold of 35-255 (CT Analyzer v1.17.0.0). The binary images were used for morphometric examination of inner-porosity, pore size, and interconnectivity.

The microstructure and nHAp composition in the fabricated scaffolds were also evaluated by micro-CT. In this case, acquisition of X-ray images was performed with a pixel size ranging from 8 to 14 µm, a rotation step of 0.6° over 360°, and a smoothing averaging of every two images, using the SkyScan acquisition software version 1.1.3. The X-ray source was fixed at 35 kV and 181 µA, of voltage and current, respectively. Following the acquisition, gray-scale images were reconstructed and, when necessary, aligned using NRecon software (version 1.7.1.0) DataViewer software (version 1.5.3.6) as previously described, respectively. Qualitative visualization of the cross-sectional morphology and the 3D polymer (black) and nano-hydroxyapatite (red) phases were obtained using CT-Vox software (version 3.3.0). Finally, two dynamic thresholds of 20-255 for the whole structure and 90-255 for the ceramic phase were applied (CT Analyzer v1.17.0.0) and used for the quantification of nHAp percentage over the polymeric composition.

Alizarin red staining of nHAp particles in 3D scaffolds: Nano-HAp content across produced scaffolds with Yarns-Threads@nHAp and Yarns-Threads/PL@nHAp was analyzed by alizarin red staining. Briefly, samples were washed with deionized water, followed by incubation with a solution of 2% (w/v) AZ (Merck) for 20 minutes under gentle shaking. Afterward, samples were thoughtfully washed with deionized water and visualized under fluorescence microscopy (Axio Imager Z1m; Zeiss).

Chemical characterization: Fourier-transform infrared spectroscopy (FTIR, A21004200704, IRPrestige 21, Shimadzu) was used for chemical analysis of the produced nanofiber threads. Briefly, prior to FTIR analysis by attenuated total reflectance (ATR), all samples without PL were dissolved with a small amount of chloroform and allowed to dry at RT to form a small pellet. In the case of samples incorporating PLs, several replicates were combined and smashed to form a small pellet. Infrared spectra of PCL and PL-incorporated yarns/threads and PLs only were recorded by averaging 32 individual scans, at a resolution of 4 cm, over a wavenumber range between 4000 and 1000 cm^{-1} at RT.

Mechanical characterization: The mechanical properties of both a A-Yarns and -PL, I-Threads and -PL and I-Threads@nHAp and -PL@nHAp were assessed using a universal mechanical testing machine (5543K2942, 5543, INSTRON) equipped with a 50N load cell. Images from optical microscope (DM750, Leica, Schweiz, Germany) were acquired and used for cross-sectional area calculations. Each specimen was measured along the length at six different locations using the ImageJ software (version 1.52d). Samples were cut into testing specimens with 2 cm and fixed in paper frames with a window of 1 × 1 cm. After mounting the frames onto the tester grips, the lateral sides were cut, and the crosshead speed was set at a constant rate of 10 mm/min. At least five samples per condition were tested. The young modulus was calculated from the tangent slope of the linear section of the stress-strain curve, and the ultimate tensile strength and load were determined by calculating the maximum of the stress-strain curve.

Water-uptake and release kinetics: Both A-Yarns and -/PL, and I-Threads and -/PL were cut into pieces (20–30 mg). To replicate both physiological and inflammatory setups, a solution of PBS (solution adjusted to pH=7.4) and PBS with sodium bicarbonate (solution adjusted to pH=6.4) were

used. At the end of each time point, samples of each formulation were collected and rinsed with distilled water (dH_2O), and the weight of the samples measured. The percentage of weight loss kinetics was calculated according to the following equation:

$$Weight\ loss = (mi - mf) \times\ 100\%.$$

Where mi is the initial weight and mf the final weight.

Cumulative release of total proteins and PLs growth factors, cytokines and chemokines: A-Yarns/PL and I-Threads/PL were collected and cut in pieces (20–30 mg) and shortly rinsed in MilliQ water. Samples were left in contact with physiological (PBS solution adjusted to pH=7.4, total volume = 1 mL) and inflammatory environments (sodium bicarbonate solution adjusted to pH=6.4, total volume =1 mL) up to 31 days at 37ºC, under 60 rpm constant agitation. At 0, 0.125, 1, 3 5 and 14 days, a total volume of 600 µl was collected. To quantitatively evaluate the cumulative release of total proteins, Pierce BCA protein assay (Micro BCATM Protein Assay Kit; Thermo Scientific™) was used according to the manufacturer protocol and measured in a microplate reader (Synergy HT, Bio-Tek Instruments). An equal volume of fresh solutions was added each time. A-Yarn and I-Thread were used as controls. Cumulative release was calculated in relation to the initial weight of samples for each tested condition.

For the cumulative release of PLs factors, after electrospinning, produced A-Yarn/PL and I-Thread/PL were maintained at 37ºC in both physiological and inflammatory environments under 60 rpm constant agitation. At 0, 0.125, 1, 3 5 and 14 days, 600 µl of solution was collected and stored at -80ºC until further analysis. An equal volume of fresh solutions was added each time. Platelet lysates GFs, cytokines and chemokines were quantitatively studied using an ELISA plate array assay. Customized ELISA plates for platelet-derived growth factor-BB (PDGF-BB), transforming growth factor beta (TGF-ß), insulin growth factor 1 (IGF-1), endothelial growth factor (EGF), vascular endothelia growth factor (VEGF), fibroblast growth factor ß (FGF-ß), RANTES and CXCL1 (Signosis, INC.) were used. Standard curves were performed for each protein ranging from 0 to 2 ng/mL. The concentration of released proteins was calculated in relation to the initial weight of samples for each tested condition and presented as ng/mL per mg of A-Yarns/PLs or I-Threads/PL.

Isolation, seeding and culture of human adipose-derived stem cells: Human stem cells from adipose source were isolated by enzymatic digestion of surplus lipoaspirate samples [66] of three healthy female patients (40–70 years old) obtained under previously established protocols with Hospital da Prelada (Porto, Portugal). All human samples were obtained under informed consent following protocols approved by the ethical committee of the hospital and according to the Declaration of Helsinki. Afterward, cells were expanded in basal medium (Alpha-MEM medium (Alfagene, Lisboa) supplemented with 10% FBS (Thermofisher, EUA) and 1% A/A (Thermofisher,EUA)). Prior to seeding, A-Yarn, I-Thread (with and without nHAp), A-Yarn/PL and I-Thread/PL (with and without nHAp), and 3D scaffolds were placed inside the 24-well plate and 12-well plate inserts (Merck, Germany), respectively, and immersed in 70% ethanol for 45 min for sterilization, followed by several washing steps with PBS for 15 min to remove the remaining ethanol residues. As a final step, samples were incubated overnight with basal medium to improve cells attachment. The following day, hASCs were seeded at a density of $3x10^4$ cells onto each sampled yarn/thread, and at a density of $30x10^4$ cells/per scaffold. Samples were afterward incubated overnight to allow cells adhesion. Fresh basal medium was added up to 0.6 mL in yarns/threads and 2 mL in 3D scaffolds, and cell were cultured for 21 days. Culture medium was changed twice a week. Cells were used at passages 2-3.

Biological characterization: cellular proliferation was evaluated using a fluorometric dsDNA quantification kit (PicoGreen; Molecular Probes, Invitrogen, Carlsbad, CA, USA) to determine DNA content. After the established culture times, hASCs-seeded fiber threads and yarns were washed twice with PBS. Then, filtered ultra-pure Millipore water (Pore size 0.22 µm) was added to subject cells to an osmotic shock. The collected cell solution was stored at -80°C to promote an additional thermal shock. After defrosting, cell lysates were used for dsDNA quantification and fluorescence was measured in a microplate reader (Synergy HT, Bio-Tek Instruments) using an excitation wavelength of 485/20 nm and an emission wavelength of 538/20 nm. Standards were prepared in a range of concentrations between 0 and 1.5 µg/mL. The fold increase was calculated using A-Yarns or I-Threads as normalizer group.

At pre-determined days, intracellular alkaline phosphatase was determined using the colorimetric n-nitrophenol (pNp) assay. Cell lysates were incubated with a substrate solution composed of 0.2%

(w/v) p-nitrophenyl phosphate (pNPP) in 1 mmol diethanolamine (Sigma-Aldrich). After incubation (1h, 37°C), a stock solution of 2 M NaOH/0.2 mM ethylenediaminetetraacetic acid was added. Absorbance was measured (405 nm) using a microplate reader (Synergy HT; Bio-Tek Instruments). A standard curve was prepared using a pNP stock solution (Sigma-Aldrich) with values ranging from 0 to 0.5 µmol/ml. The fold increase was calculated using A-Yarns and I-Threads as normalizer group.

Matrix mineralization: Matrix mineralization was analyzed by alizarin red staining in hASCs-seeded threads (with and without nHAp) after 5 and 15 days, and in scaffolds after 14 days of culture. Briefly, samples were washed with deionized water, followed by incubation with a solution of 2% (w/v) AZ (Merck) for 20 minutes under gentle shaking. Afterward, samples were thoughtfully washed with deionized water and analyzed under a stereomicroscope (Discovery v8, Zeiss, Deutschland, Germany) and images acquired with AxioCam ICC1 (Zeiss, Germany).

Immunofluorescence of tendon-, bone- and interface-related markers: Seeded yarns/threads (with and without PL) and gradient scaffolds were fixed with 10% (v/v) neutral buffered formalin for 20 minutes at RT. Briefly, to assess the expression of tenogenic and extracellular matrix (ECM) related markers in Yarns-Plain/PLs and Iso-Plain/PLs, and the expression of tenogenic-, osteogenic- and interface-related markers in 3D scaffolds, samples were first washed with PBS and permeabilized with 0.25% Triton X-100/PBS solution for 30 minutes. To block non-specific binding, a solution of 1% bovine serum albumin (w/v, BSA, Thermofisher, EUA) in PBS was added and left for 30 minutes at RT. Afterward, A-Yarn, A-Yarn/PL, I-Thread and I-Thread/PL were incubated with anti-Scleraxis antibody (rabbit anti-human SCX 1:100; Abcam) and anti-Collagen type III (rabbit anti-human COLIII, 1:500, Abcam) overnight at 4 °C with gentle shaking. In the case of 3D scaffolds, samples were incubated with anti-SRY-Box Transcription Factor 9 (mouse anti-human SOX9, 1:200, Millipore) and anti-collagen II (rabbit anti-human COLII, 1:100, Abcam) overnight at 4 °C with gentle shaking. After incubation with the primary antibody, mouse anti-rabbit AlexaFluor 488, goat anti-rabbit AlexaFluor 594 and donkey anti-mouse AlexaFluor 488 were used secondary antibody. All antibodies were diluted in 1% (w/v) BSA. Cell nuclei and cytoskeleton were counterstained with 4,6-diamidino-2-phenyindole dilactate (DAPI, 1:1000, Thermofisher, EUA) and phalloidin solution (PHA, 1:200, Merck, Germany), respectively.

In the case of yarns/threads, samples were visualized and images acquired using a fluorescence microscopy (Axio Imager Z1m; Zeiss), while 3D scaffolds were visualized and images acquired by confocal laser scanning microscopy (Leica TCS SP8, Microsystems, Wetzlar, Germany).

Nuclei colocalization: First fluorescence images were split in different acquired channels, being only analyzed the green and blue channels of the data set. Using the plugin "colocalization" of Image J, the correlation of pixel intensities, where the two channels were "colocalized," was given. Afterwards, obtained 8-bit colocalized images were quantified, as well as, the green channel intensity and nuclei colocalization percentage determined for each yarns/threads and culture time. Three independent experiments (n = 3) were performed and a total of five images analyzed.

Statistical analysis: Results are presented as mean ± standard deviation (SD) if not stated otherwise. Statistical analyses were performed using GraphPad Prism 8.4.0 software. Two-way analysis of variance (ANOVA) with Sidak and Tukey tests was used. Nonparametric *t*-test (Mann-Whitney test) and unpaired *t*-test were performed for mechanical tensile testing. Differences between experimental groups were considered significant, with a confidence interval of 95%, whenever $p<0.05$.

Supporting Information

Supporting Information is available from the Wiley Online Library or from the author.

Acknowledgements

The authors would like to thank to Hospital da Prelada (Porto, Portugal) for the lipoaspirate tissue samples (Plastic Surgery Department). The authors acknowledge the financial support from the European Union Framework Programme for Research and Innovation HORIZON2020, Achilles (810850) and ERC CoG MagTendon (772817), and Fundação para a Ciência e a Tecnologia for MagTT

(029930) and SmarTendon (PTDC/NAN-MAT/30595/2017) projects and the PhD grant of IC (PD/BD/128088/2016).

Received: ((will be filled in by the editorial staff))
Revised: ((will be filled in by the editorial staff))
Published online: ((will be filled in by the editorial staff))

References

[1] a) I. Calejo, R. Costa-Almeida, R. L. Reis, M. E. Gomes, *Tissue Eng Part B Rev* **2019**, 25, 330; b) S. Thomopoulos, G. R. Williams, J. A. Gimbel, M. Favata, L. J. Soslowsky, *Journal of Orthopaedic Research* **2003**, 21, 413.

[2] C. C. Kaeding, B. Aros, A. Pedroza, E. Pifel, A. Amendola, J. T. Andrish, W. R. Dunn, R. G. Marx, E. C. McCarty, R. D. Parker, R. W. Wright, K. P. Spindler, *Sports Health* **2011**, 3, 73.

[3] a) G. Gasbarro, J. Ye, H. Newsome, K. Jiang, V. Wright, D. Vyas, J. J. Irrgang, V. Musahl, *Arthroscopy* **2016**, 32, 1947; b) N. N. Verma, W. Dunn, R. S. Adler, F. A. Cordasco, A. Allen, J. MacGillivray, E. Craig, R. F. Warren, D. W. Altchek, *Arthroscopy* **2006**, 22, 587.

[4] J. M. Lowen, J. K. Leach, *Advanced Functional Materials* **2020**, 30, 1909089.

[5] a) Y. Jun, E. Kang, S. Chae, S.-H. Lee, *Lab on a Chip* **2014**, 14, 2145; b) X.-Y. Du, Q. Li, G. Wu, S. Chen, *Advanced Materials* **2019**, 31, 1903733.

[6] a) M. E. Gomes, H. S. Azevedo, A. R. Moreira, V. Ellä, M. Kellomäki, R. L. Reis, *Journal of Tissue Engineering and Regenerative Medicine* **2008**, 2, 243; b) M. L. Muerza-Cascante, D. Haylock, D. W. Hutmacher, P. D. Dalton, *Tissue Engineering Part B: Reviews* **2014**, 21, 187.

[7] a) D. Puppi, F. Chiellini, *Polymer International* **2017**, 66, 1690; b) I. Calejo, R. Costa-Almeida, R. L. Reis, M. E. Gomes, *Advanced Healthcare Materials* **2019**, 8, 1900200.

[8] a) R. F. Canadas, J. M. Cavalheiro, J. D. Guerreiro, M. C. de Almeida, E. Pollet, C. L. da Silva, M. M. da Fonseca, F. C. Ferreira, *Int J Biol Macromol* **2014**, 71, 131; b) N. Nagiah, C. J. Murdock, M. Bhattacharjee, L. Nair, C. T. Laurencin, *Scientific Reports* **2020**, 10, 609.

[9] X. Wang, B. Ding, B. Li, *Mater Today (Kidlington)* **2013**, 16, 229.

[10] a) A. R. Tomás, A. I. Gonçalves, E. Paz, P. Freitas, R. M. A. Domingues, M. E. Gomes, *Nanoscale* **2019**, 11, 18255; b) M. Laranjeira, R. M. A. Domingues, R. Costa-Almeida, R. L. Reis, M. E. Gomes, *Small* **2017**, 13, 1700689.

[11] K. L. Moffat, A. S. Kwei, J. P. Spalazzi, S. B. Doty, W. N. Levine, H. H. Lu, *Tissue Eng Part A* **2009**, 15, 115.

[12] a) G. Criscenti, A. Longoni, A. Di Luca, C. De Maria, C. A. van Blitterswijk, G. Vozzi, L. Moroni, *Biofabrication* **2016**, 8, 015009; b) H. Chen, D. F. Baptista, G. Criscenti, J. Crispim, H. Fernandes, C. van Blitterswijk, R. Truckenmüller, L. Moroni, *Nanoscale* **2019**, 11, 14312; c) X. Jiang, S. Wu, M. Kuss, Y. Kong, W. Shi, P. N. Streubel, T. Li, B. Duan, *Bioactive Materials* **2020**, 5, 636; d) S. B. Orr, A. Chainani, K. J. Hippensteel, A. Kishan, C. Gilchrist, N. W. Garrigues, D. S. Ruch, F. Guilak, D. Little, *Acta Biomaterialia* **2015**, 24, 117.

[13] M. Buzgo, A. Mickova, M. Rampichova, M. Doupnik, in *Core-Shell Nanostructures for Drug Delivery and Theranostics*, DOI: 10.1016/B978-0-08-102198-9.00011-9 (Eds: M. L. Focarete, A. Tampieri), Woodhead Publishing **2018**, p. 325.

[14] D. Han, A. J. Steckl, *ChemPlusChem* **2019**, 84, 1453.

[15] a) M. Li, Y. Zheng, B. Xin, Y. Xu, *Industrial & Engineering Chemistry Research* **2020**, 59, 6301; b) H. Jiang, Y. Hu, P. Zhao, Y. Li, K. Zhu, *Journal of Biomedical Materials Research Part B: Applied Biomaterials* **2006**, 79B, 50.

[16] N. Nikmaram, S. Roohinejad, S. Hashemi, M. Koubaa, F. J. Barba, A. Abbaspourrad, R. Greiner, *RSC Advances* **2017**, 7, 28951.

[17] A. C. Mitchell, P. S. Briquez, J. A. Hubbell, J. R. Cochran, *Acta biomaterialia* **2016**, 30, 1.

[18] a) H. Zhang, K. Wang, T. Gao, R. Zhang, Z. Cai, J. Liu, H. Ma, W. Zhang, *Biomedical Materials* **2020**, 15, 035021; b) J. Hu, Y. Song, C. Zhang, W. Huang, A. Chen, H. He, S. Zhang, Y. Chen, C. Tu, J. Liu, X. Xuan, Y. Chang, J. Zheng, J. Wu, *ACS Applied Bio Materials* **2020**, 3, 965; c) O. Evrova, G. M. Burgisser, C. Ebnother, A. Adathala, M. Calcagni, E. Bachmann, J. G. Snedeker, C. Scalera, P. Giovanoli, V. Vogel, J. Buschmann, *Biomaterials* **2020**, 232, 119722.

[19] E. Anitua, M. Sánchez, G. Orive, *Advanced Drug Delivery Reviews* **2010**, 62, 741.

[20] a) E. Anitua, M. Sánchez, A. T. Nurden, P. Nurden, G. Orive, I. Andía, *Trends in Biotechnology* **2006**, 24, 227; b) N. Fekete, M. Gadelorge, D. Fürst, C. Maurer, J. Dausend, S. Fleury-Cappellesso, V. Mailänder, R. Lotfi, A. Ignatius, L. Sensebé, P. Bourin, H. Schrezenmeier, M. T. Rojewski, *Cytotherapy* **2012**, 14, 540.

[21] a) B. B. Mendes, M. Gómez-Florit, P. S. Babo, R. M. Domingues, R. L. Reis, M. E. Gomes, *Advanced Drug Delivery Reviews* **2018**, 129, 376; b) S. C. N. d. S. Santos, Ó. E. Sigurjonsson, C. d. A. Custódio, J. F. C. d. L. Mano, *Tissue Eng Part B Rev* **2018**, 24, 454.

[22] a) R. Yonemitsu, T. Tokunaga, C. Shukunami, K. Ideo, H. Arimura, T. Karasugi, E. Nakamura, J. Ide, Y. Hiraki, H. Mizuta, *The American Journal of Sports Medicine* **2019**, 47, 1701; b) C. C. Würgler-Hauri, L. M. Dourte, T. C. Baradet, G. R. Williams, L. J. Soslowsky, *J Shoulder Elbow Surg* **2007**, 16, S198; c) Y. Huang, M. Pan, H. Shu, B. He, F. Zhang, L. Sun, *Journal of Cellular Biochemistry* **2020**, 121, 2343; d) S. Yamazaki, K. Yasuda, F. Tomita, H. Tohyama, A. Minami, *Arthroscopy* **2005**, 21, 1034; e) A. Weiler, C. Förster, P. Hunt, R. Falk, T. Jung, F. N. Unterhauser, V. Bergmann, G. Schmidmaier, N. P. Haas, *Am J Sports Med* **2004**, 32, 881.

[23] a) B. Edderkaoui, *Front Endocrinol (Lausanne)* **2017**, 8, 39; b) A. Stålman, D. Bring, P. W. Ackermann, *Knee Surg Sports Traumatol Arthrosc* **2015**, 23, 2682.

[24] N. Felsenthal, E. Zelzer, *Development* **2017**, 144, 4271.

[25] a) J. Lee, A. A. Abdeen, K. A. Kilian, *Scientific Reports* **2014**, 4, 5188; b) I. Calejo, R. Costa-Almeida, R. L. Reis, M. E. Gomes, *Trends in Biotechnology* **2020**, 38, 83.

[26] a) L. Krishna, K. Dhamodaran, C. Jayadev, K. Chatterjee, R. Shetty, S. S. Khora, D. Das, *Stem Cell Research & Therapy* **2016**, 7, 188; b) R. Ravichandran, S. Liao, C. C. Ng, C. K. Chan, M. Raghunath, S. Ramakrishna, *World J Stem Cells* **2009**, 1, 55.

[27] a) S. P. Magnusson, K. Qvortrup, J. O. Larsen, S. Rosager, P. Hanson, P. Aagaard, M. Krogsgaard, M. Kjaer, *Matrix Biol* **2002**, 21, 369; b) P. Kannus, *Scand J Med Sci Sports* **2000**, 10, 312.

[28] S. Von Euw, Y. Wang, G. Laurent, C. Drouet, F. Babonneau, N. Nassif, T. Azaïs, *Scientific Reports* **2019**, 9, 8456.

[29] a) E. A. McNally, H. P. Schwarcz, G. A. Botton, A. L. Arsenault, *PLOS ONE* **2012**, 7, e29258; b) A. Boyde, *Methods Mol Biol* **2019**, 1914, 571.

[30] a) R. Pal, *AIChE Journal* **1996**, 42, 3181; b) F. L. Román, M. Schmidt, H. Löwen, *Physical Review E* **2000**, 61, 5445.

[31] M. Buzgo, M. Rampichova, K. Vocetkova, V. Sovkova, V. Lukasova, M. Doupnik, A. Mickova, F. Rustichelli, E. Amler, *RSC Advances* **2017**, 7, 1215.

[32] S. Damodaran, *Journal of Food Science* **2005**, 70, R54.

[33] a) E. Bouyer, G. Mekhloufi, V. Rosilio, J.-L. Grossiord, F. Agnely, *International Journal of Pharmaceutics* **2012**, 436, 359; b) D. J. McClements, *Food Emulsions: Principles, Practices, and Techniques*, CRC Press, **2004**; c) D. J. Burgess, O. N. Sahin, *Pharm Dev Technol* **1998**, 3, 21.

[34] X. Xu, X. Zhuang, X. Chen, X. Wang, L. Yang, X. Jing, *Macromolecular Rapid Communications* **2006**, 27, 1637.

[35] P. Lu, Y. Xia, *Langmuir* **2013**, 29, 7070.

[36] a) Ş. Şeker, A. E. Elçin, Y. M. Elçin, *Journal of Materials Science: Materials in Medicine* **2019**, 30, 127; b) S. A. Bernal-Chávez, S. Alcalá-Alcalá, D. Cerecedo, A. Ganem-Rondero, *European Journal of Pharmaceutical Sciences* **2020**, 146, 105231.

[37] a) A. Camerlo, A. M. Bühlmann-Popa, C. Vebert-Nardin, R. M. Rossi, G. Fortunato, *Journal of Materials Science* **2014**, 49, 8154; b) F. Cengiz Çallıoğlu, H. Kesici Güler, E. Sesli Çetin, *Materials Research Express* **2019**, 6, 125013.

[38] J. Wu, Y. Hong, *Bioactive Materials* **2016**, 1, 56.

[39] A. S. LaCroix, S. E. Duenwald-Kuehl, R. S. Lakes, R. Vanderby, Jr., *J Appl Physiol (1985)* **2013**, 115, 43.

[40] A. S. Deshpande, P.-A. Fang, X. Zhang, T. Jayaraman, C. Sfeir, E. Beniash, *Biomacromolecules* **2011**, 12, 2933.

[41] M. Carles-Carner, L. S. Saleh, S. J. Bryant, *Biomed Mater* **2018**, 13, 045009.

[42] R. Kang, Y. Luo, L. Zou, L. Xie, H. Lysdahl, X. Jiang, C. Chen, L. Bolund, M. Chen, F. Besenbacher, C. Bünger, *RSC Advances* **2014**, 4, 5734.

[43] H. Chen, X. Huang, M. Zhang, F. Damanik, M. B. Baker, A. Leferink, H. Yuan, R. Truckenmüller, C. van Blitterswijk, L. Moroni, *Acta Biomaterialia* **2017**, 59, 82.

[44] J. C. Berkmann, A. X. Herrera Martin, A. Ellinghaus, C. Schlundt, H. Schell, E. Lippens, G. N. Duda, S. Tsitsilonis, K. Schmidt-Bleek, *Int J Mol Sci* **2020**, 21.

[45] B. S. Sørensen, M. Busk, J. Overgaard, M. R. Horsman, J. Alsner, *PLOS ONE* **2015**, 10, e0134955.

[46] M. Chen, C. Chen, Z. Shen, X. Zhang, Y. Chen, F. Lin, X. Ma, C. Zhuang, Y. Mao, H. Gan, P. Chen, X. Zong, R. Wu, *Oncotarget* **2017**, 8, 45759.

[47] A. Raza, T. Rasheed, F. Nabeel, U. Hayat, M. Bilal, H. M. N. Iqbal, *Molecules* **2019**, 24, 1117.

[48] L. Macdougall, H. Culver, C.-C. Lin, C. Bowman, K. Anseth, in *Biomaterials Science (Fourth Edition)*, DOI: 10.1016/B978-0-12-816137-1.00015-5 (Eds: W. R. Wagner, S. E. Sakiyama-Elbert, G. Zhang, M. J. Yaszemski), Academic Press **2020**, p. 167.

[49] J. M. Anderson, A. Rodriguez, D. T. Chang, *Seminars in Immunology* **2008**, 20, 86.

[50] S. Font Tellado, E. R. Balmayor, M. Van Griensven, *Advanced Drug Delivery Reviews* **2015**, 94, 126.

[51] F. Ng, S. Boucher, S. Koh, K. S. R. Sastry, L. Chase, U. Lakshmipathy, C. Choong, Z. Yang, M. C. Vemuri, M. S. Rao, V. Tanavde, *Blood* **2008**, 112, 295.

[52] T. Molloy, Y. Wang, G. Murrell, *Sports Med* **2003**, 33, 381.

[53] a) Z. Mihaylova, R. Tsikandelova, P. Sanimirov, N. Gateva, V. Mitev, N. Ishkitiev, *Archives of Oral Biology* **2018**, 85, 1; b) A. Colciago, F. Celotti, L. Casati, R. Giancola, S. M. Castano, G. Antonini, M. C. Sacchi, P. Negri-Cesi, *Int J Biomed Sci* **2009**, 5, 380.

[54] S. P. B. Teixeira, R. M. A. Domingues, M. Shevchuk, M. E. Gomes, N. A. Peppas, R. L. Reis, *Advanced Functional Materials* **2020**, 30, 1909011.

[55] a) A. I. Gonçalves, M. T. Rodrigues, S. J. Lee, A. Atala, J. J. Yoo, R. L. Reis, M. E. Gomes, *PLoS One* **2013**, 8, e83734; b) S. M. Mihaila, A. K. Gaharwar, R. L. Reis, A. Khademhosseini, A. P. Marques, M. E. Gomes, *Biomaterials* **2014**, 35, 9087.

[56] J. R. Farley, D. J. Baylink, *Metabolism - Clinical and Experimental* **1986**, 35, 563.

[57] Y. Yoshimoto, A. Takimoto, H. Watanabe, Y. Hiraki, G. Kondoh, C. Shukunami, *Scientific Reports* **2017**, 7, 45010.

[58] N. D. Murchison, B. A. Price, D. A. Conner, D. R. Keene, E. N. Olson, C. J. Tabin, R. Schweitzer, *Development* **2007**, 134, 2697.

[59] S. W. Volk, S. R. Shah, A. J. Cohen, Y. Wang, B. K. Brisson, L. K. Vogel, K. D. Hankenson, S. L. Adams, *Calcif Tissue Int* **2014**, 94, 621.

[60] H. A. Eriksen, A. Pajala, J. Leppilahti, J. Risteli, *Journal of Orthopaedic Research* **2002**, 20, 1352.

[61] Y. Mikuni-Takagaki, Y. Kakai, M. Satoyoshi, E. Kawano, Y. Suzuki, T. Kawase, S. Saito, *J Bone Miner Res* **1995**, 10, 231.

[62] S. Wu, Y. Wang, P. N. Streubel, B. Duan, *Acta Biomater* **2017**, 62, 102.

[63] L. Rossetti, L. A. Kuntz, E. Kunold, J. Schock, K. W. Müller, H. Grabmayr, J. Stolberg-Stolberg, F. Pfeiffer, S. A. Sieber, R. Burgkart, A. R. Bausch, *Nature Materials* **2017**, 16, 664.

[64] M. Benjamin, H. Toumi, J. R. Ralphs, G. Bydder, T. M. Best, S. Milz, *J Anat* **2006**, 208, 471.

[65] R. Costa-Almeida, I. Calejo, R. Altieri, R. M. A. Domingues, E. Giordano, R. L. Reis, M. E. Gomes, *Biomedical Materials* **2019**, 14, 034104.

[66] P. P. Carvalho, X. Wu, G. Yu, I. R. Dias, M. E. Gomes, R. L. Reis, J. M. Gimble, *Cells Tissues Organs* **2011**, 194, 494.

Texturing hierarchical tissues by gradient assembling of microengineered platelet-lysates activated fibers

Isabel Calejo, Rui L. Reis, Rui M. A. Domingues, Manuela E. Gomes**

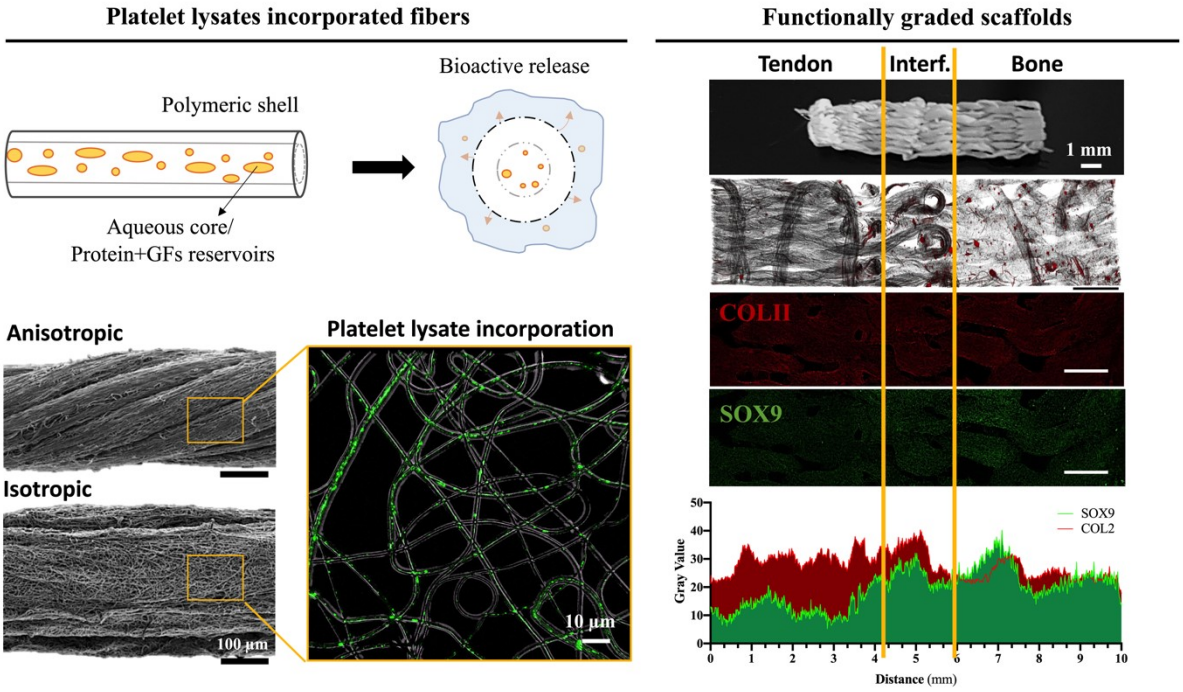

Functionally graded 3D scaffolds are produced by emulsion electrospinning and textile assembling. A-Yarns/PL induced anisotropic cellular alignment and high expression of SCX, resembling tendon tissue microenvironment. I-Threads/PL@nHAp trigger a high deposition of mineralized matrix in culture suggesting an osteogenic commitment. The textile assembling of bioactive core-shell fiber enabled the production of a biochemical, biological and tissue-engineered gradient in PL-functional 3D gradient constructs.